Computer Methods in Applied Mechanics and Engineering 427 (2024) 117059

Contents lists available at ScienceDirect

Comput. Methods Appl. Mech. Engrg.

journal homepage: www.elsevier.com/locate/cma

A general ordinary state-based peridynamic formulation for anisotropic materials

Francesco Scabbia [a,*], Mirco Zaccariotto [a,b], Ugo Galvanetto [a,b]

[a] Department of Industrial Engineering, University of Padova, via Venezia 1, Padova, 35131, Italy
[b] Center of Studies and Activities for Space (CISAS) - "G. Colombo", via Venezia 15, Padova, 35131, Italy

ARTICLE INFO

Keywords:
Peridynamics
Anisotropic material
Orthotropic material
Micromoduli
Bond orientation
Numerical implementation

ABSTRACT

A general ordinary state-based peridynamic formulation to model anisotropic materials in 2D and 3D is proposed. The new peridynamic constitutive model introduces two bond stiffness functions depending on the bond orientations. These functions are defined such that the components of the elasticity tensor evaluated by using the new formulation exactly reproduce those of classical continuum mechanics in the case of homogeneous deformation. Several numerical examples in 2D and 3D illustrate the validity of the proposed formulation for fully anisotropic materials. This formulation is also suitable to model monoclinic, orthotropic, transversely isotropic, and isotropic materials.

1. Introduction

Engineers often approximate the constitutive behavior of materials with the assumption of isotropic properties. However, most materials are intrinsically anisotropic due to the asymmetry in the arrangement of atoms, molecules, or microstructures, exhibiting distinct physical and mechanical characteristics at the macro-scale when measured along different directions [1]. The broad class of anisotropic materials embeds both natural materials, such as bones [2], woods [3] and rocks [4], and artificial materials, such as composites [5]. In particular, advanced composite materials are frequently used in many aerospace applications to exploit their superior (even if anisotropic) mechanical properties. Isotropic materials may also present anisotropic responses due to some manufacturing processes, like the cold-rolling of aluminum [6]. Furthermore, the initiation and propagation of cracks may also be influenced by the anisotropic properties of the material, such as in the failure of composites [7] and the bone fracture [8–10].

Peridynamics (PD) is a nonlocal continuum theory devised to model fracture phenomena [11,12]. This theory is able to predict realistic crack paths that are closer to experimental observations if compared with other numerical methods based on classical continuum mechanics (CCM), such as the interface elements with cohesive zone modeling [13], the extended finite element method (XFEM) [13], and the phase field model [14]. Bond-based peridynamics [11] was the first version of the peridynamic theory in which the material points interact through long-range forces with the same orientation and magnitude, as shown in Fig. 1(a). The interaction between two points is called *bond*. This formulation restricts the value of the Poisson's ratio to $1/4$ in 3D and in plane strain conditions, and to $1/3$ in plane stress conditions [15]. The state-based version of the peridynamic theory [12] allows to overcome this limitation since the force that one point exerts on another may be different from the force that the second point exerts on the first one. Furthermore, this new formulation can be subdivided into *ordinary* and *non-ordinary* state-based peridynamics, in which the force is aligned and unaligned to the bond direction, respectively (see Figs. 1(b) and 1(c)).

* Corresponding author.
E-mail addresses: francesco.scabbia@unipd.it (F. Scabbia), mirco.zaccariotto@unipd.it (M. Zaccariotto), ugo.galvanetto@unipd.it (U. Galvanetto).

https://doi.org/10.1016/j.cma.2024.117059
Received 5 March 2024; Received in revised form 7 May 2024; Accepted 10 May 2024
Available online 24 May 2024

(a) *Bond-based PD.* (b) *Ordinary state-based PD.* (c) *Non-ordinary state-based PD.*

Fig. 1. Interaction forces for the three different versions of the peridynamic theory.

Peridynamics has been used to predict fracture phenomena (see, for example, [16–21]), or to solve multi-physics problems involving fracture, such as thermo-mechanical problems [22–24], corrosion [25–27], piezoelectricity [28,29], and oxidation phenomena [30–33]. However, most of these applications adopted the assumption of isotropic materials. Bond-based peridynamics was generalized to model composites [34–41] or materials with some degree of anisotropy [42–46] by modifying the bond force as a function of its direction. However, since the bond force is defined by a pair potential function in the bond-based formulation, the elastic coefficients must satisfy the Cauchy's relations and some of them have a fixed value [45]. Therefore, bond-based peridynamics is not suitable to model fully anisotropic media.

Apart from the state-based formulation of the peridynamic theory, other methods have been developed to overcome these limitation on the elastic coefficients. The continuum-kinematics-inspired peridynamics [47,48] reformulates the interactions between points such that the nonlocal kinematics coincide with that of classical continuum kinematics, capturing the Poisson's effect correctly in isotropic materials. This formulation was generalized for 2D orthotropic and 3D transversely isotropic materials [49], but still the values of some elastic coefficients are fixed a priori. Another method to overcome the Poisson's ratio limitation in peridynamic isotropic media is to add shear deformability to the bond-based formulation by introducing the rotational degrees of freedom at the peridynamic points [50–52], and this allows to model the proper stiffness characteristics of orthotropic materials as well [53,54]. However, the inclusion of new degrees of freedom in the peridynamic framework increases the complexity and the computational cost of the numerical simulations. The authors of [55] recast the peridynamic equations by using the peridynamic operator method to model 2D anisotropic materials.

Ordinary state-based peridynamics was used to model 2D orthotropic media by introducing two new bond stiffness coefficients along the two principal axes of the material [56], but the off-axis stiffness exhibits different values with respect to that obtained with classical continuum mechanics. Furthermore, this method cannot be easily generalized to 3D models. Non-ordinary state-based peridynamics allows one to incorporate constitutive models directly from classical continuum mechanics, i.e., without the calibration of peridynamic properties to the classical ones [12]. These types of models are often called *peridynamic correspondence models*. Therefore, several non-ordinary state-based peridynamic models were developed to simulate anisotropic material properties [57–61]. Nevertheless, non-ordinary state-based peridynamics suffer from instability issues, such as zero-energy modes, and these models require additional stabilization techniques to obtain reasonable numerical results [62–64].

In this work, we propose a new ordinary state-based formulation of the peridynamic theory able to model fully anisotropic, linear elastic materials both in 2D and 3D. We introduce two micromoduli, i.e., the bond stiffness properties, that depend on the bond orientations. These micromoduli are defined such that all the components of the CCM elasticity tensor are exactly reproduced by the peridynamic constitutive laws, without any limitations on their values. This new formulation is verified by several numerical examples in 2D and 3D. The formulation presented in this paper is the first step towards the possibility to use PD to describe the fracture behavior of anisotropic materials.

The paper is structured as follows. Sections 2 and 3 review the classical constitutive model for anisotropic linear elastic materials and the ordinary state-based peridynamic formulation for isotropic materials, respectively. Section 4 proposes the new peridynamic formulation for anisotropic materials based on the definition of two micromoduli depending on the bond orientation. Section 5 describes the numerical implementation of the new formulation and Section 6 shows the numerical results of several 2D and 3D examples. Section 7 draws the conclusions of the work.

2. Classical constitutive model for linear elastic materials

In classical continuum mechanics, the constitutive model for a linear elastic material with an initial unstressed configuration is given by the generalized Hooke's law [5] as

$$\sigma_{ij} = C_{ijk\ell}\,\varepsilon_{k\ell}\,, \tag{1}$$

where σ_{ij} are the components of the 2nd-order stress tensor, $C_{ijk\ell}$ are the components of the 4th-order elasticity tensor, and $\varepsilon_{k\ell}$ are the components of the 2nd-order strain tensor. In Eq. (1) Einstein summation convention for repeated indices is used.

The symmetry of the stress and strain tensors is inherited by the elasticity tensor, which exhibits the so-called *minor symmetries*:

$$C_{ijk\ell} = C_{jik\ell} = C_{ij\ell k}\,. \tag{2}$$

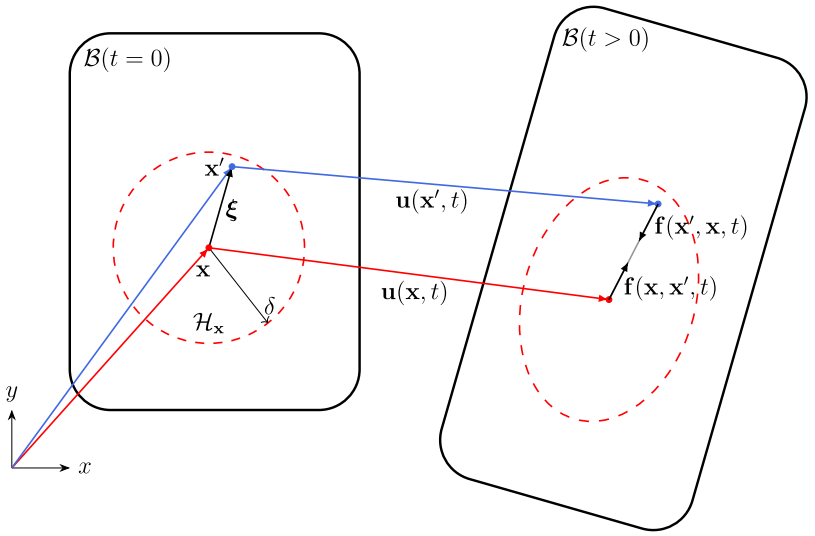

Fig. 2. Body modeled with peridynamics in the reference configuration $\mathcal{B}(t=0)$ and deformed configuration $\mathcal{B}(t>0)$.

Furthermore, since $C_{ijk\ell}$ can be derived as a double derivative of the strain energy density W with respect to the strain components [5], the elasticity tensor also has the so-called *major symmetries*:

$$C_{ijk\ell} = \frac{\partial^2 W}{\partial \varepsilon_{ij}\,\partial \varepsilon_{k\ell}} = \frac{\partial^2 W}{\partial \varepsilon_{k\ell}\,\partial \varepsilon_{ij}} = C_{k\ell ij}\,. \tag{3}$$

The Cauchy's relations [65] impose a further symmetry to the elasticity tensor:

$$C_{ijk\ell} = C_{ikj\ell}\,. \tag{4}$$

If a material meets the conditions in Eq. (4), such as a material described by a pair potential function, then the elasticity tensor is completely symmetric, i.e., the value of an elastic coefficient $C_{ijk\ell}$ is the same when arbitrarily switching the order of the indices i, j, k, and ℓ [45,65]. However, real materials rarely satisfy the Cauchy's relations.

3. Ordinary state-based peridynamics for isotropic materials

The equation of motion at a point $\mathbf{x}$ at time $t \geq 0$ in a body $\mathcal{B}$ modeled with peridynamics is given by [11,12]

$$\rho(\mathbf{x})\,\ddot{\mathbf{u}}(\mathbf{x},t) = \int_{\mathcal{H}_{\mathbf{x}}} \mathbf{f}(\mathbf{x},\mathbf{x}',t)\mathrm{d}V_{\mathbf{x}'} + \mathbf{b}(\mathbf{x},t)\,, \tag{5}$$

where ρ is the density of the material, $\ddot{\mathbf{u}}$ is the acceleration field, $\mathbf{f}$ is the bond force (force per unit volume squared), $\mathcal{H}_{\mathbf{x}}$ is the integration region around point $\mathbf{x}$, $V_{\mathbf{x}'}$ is the volume of a point $\mathbf{x}'$ within $\mathcal{H}_{\mathbf{x}}$, and $\mathbf{b}$ is the external force density. Fig. 2 shows the bond forces arising within a bond due to the deformation of a body modeled with peridynamics. The interaction between $\mathbf{x}$ and $\mathbf{x}'$ is named *bond* and is defined as $\boldsymbol{\xi} = \mathbf{x}' - \mathbf{x}$. The integration region $\mathcal{H}_{\mathbf{x}}$, called the *neighborhood*, is often chosen to be a circle in 2D and a sphere in 3D with a radius δ, named *horizon size*: $\mathcal{H}_{\mathbf{x}} = \left\{ \mathbf{x}' \in \mathcal{B}(t=0) \,:\, \|\boldsymbol{\xi}\| \leq \delta \right\}$. Under static conditions, the peridynamic equation is simplified as

$$-\int_{\mathcal{H}_{\mathbf{x}}} \mathbf{f}(\mathbf{x},\mathbf{x}')\mathrm{d}V_{\mathbf{x}'} = \mathbf{b}(\mathbf{x})\,. \tag{6}$$

In state-based peridynamics [12], the bond force is defined as

$$\mathbf{f}(\mathbf{x},\mathbf{x}',t) = \underline{\mathbf{T}}[\mathbf{x},t]\langle\boldsymbol{\xi}\rangle - \underline{\mathbf{T}}[\mathbf{x}',t]\langle-\boldsymbol{\xi}\rangle\,, \tag{7}$$

where $\underline{\mathbf{T}}$ is the *force density vector state*. By convention, the variables the state depends on are denoted within square brackets $[\cdot]$, whereas the bond the state is applied to is denoted within angle brackets $\langle\cdot\rangle$. Where possible, we will omit the square brackets. Note that $\underline{\mathbf{T}}[\mathbf{x},t]\langle\boldsymbol{\xi}\rangle$ and $\underline{\mathbf{T}}[\mathbf{x}',t]\langle-\boldsymbol{\xi}\rangle$ may have different magnitudes, as shown in Fig. 1(b).

For later use, the *reference position scalar state* and the *displacement vector state* [12,66] are respectively defined as

$$\underline{x}\langle\boldsymbol{\xi}\rangle = \|\boldsymbol{\xi}\|\,, \tag{8}$$

$$\underline{\mathbf{U}}[\mathbf{x},t]\langle\boldsymbol{\xi}\rangle = \mathbf{u}(\mathbf{x}',t) - \mathbf{u}(\mathbf{x},t)\,, \tag{9}$$

where $\mathbf{u}$ is a displacement field applied to the body $\mathcal{B}$. To describe the axial elongation of the bond, the *extension scalar state* is defined as

$$\underline{e}[\mathbf{x},t]\langle\boldsymbol{\xi}\rangle = \|\boldsymbol{\xi}+\underline{\mathbf{U}}\langle\boldsymbol{\xi}\rangle\| - \|\boldsymbol{\xi}\| \,. \tag{10}$$

The *direction vector state*, or the unit vector state in the direction of the deformed bond is defined as

$$\underline{\mathbf{M}}[\mathbf{x},t]\langle\boldsymbol{\xi}\rangle = \frac{\boldsymbol{\xi}+\underline{\mathbf{U}}\langle\boldsymbol{\xi}\rangle}{\|\boldsymbol{\xi}+\underline{\mathbf{U}}\langle\boldsymbol{\xi}\rangle\|} \,. \tag{11}$$

The integral of the product of two scalar states $\underline{a}$ and $\underline{b}$ can be denoted as

$$\underline{a} \bullet \underline{b} = \int_{\mathcal{H}_\mathbf{x}} \underline{a}\langle\boldsymbol{\xi}\rangle \, \underline{b}\langle\boldsymbol{\xi}\rangle \mathrm{d}V_{\mathbf{x}'} \,. \tag{12}$$

This notation allows to highlight the peridynamic "structure" of the following formulae. The *weighted volume* at a point $\mathbf{x}$ is defined as

$$\begin{aligned} m(\mathbf{x}) &= \int_{\mathcal{H}_\mathbf{x}} \underline{\omega}\langle\boldsymbol{\xi}\rangle \, \|\boldsymbol{\xi}\|^2 \mathrm{d}V_{\mathbf{x}'} \\ &= (\underline{\omega}\,\underline{x}) \bullet \underline{x} \,, \end{aligned} \tag{13}$$

where $\underline{\omega}$ is a scalar state called *influence function*. In this work, we adopt the Gaussian influence function: $\underline{\omega}\langle\boldsymbol{\xi}\rangle = \underline{\omega}(\|\boldsymbol{\xi}\|) = \exp(-\|\boldsymbol{\xi}\|^2/\delta^2)$ [67]. It is worth noting that the choice of a different influence function may (slightly) change the peridynamic solution, but it does not affect the validity of the theory presented in this work. The dilatation at a point $\mathbf{x}$ is defined as

$$\begin{aligned} \theta(\mathbf{x},t) &= \frac{c_\theta}{m} \int_{\mathcal{H}_\mathbf{x}} \underline{\omega}(\|\boldsymbol{\xi}\|) \, \|\boldsymbol{\xi}\| \, \underline{e}\langle\boldsymbol{\xi}\rangle \mathrm{d}V_{\mathbf{x}'} \\ &= \frac{c_\theta}{m} (\underline{\omega}\,\underline{x}) \bullet \underline{e} \,, \end{aligned} \tag{14}$$

where c_θ is the dilatation coefficient that is calibrated by equalizing θ and the CCM value of the dilatation in an infinite body under homogeneous deformation: $c_\theta = 3$ in 3D, $c_\theta = 2$ in 2D plane strain conditions, and $c_\theta = 2(1-2\nu)/(1-\nu)$ in 2D plane stress conditions [12,68]. Similarly to classical continuum mechanics, the *deviatoric extension scalar state* of a bond is defined as

$$\underline{e}^d[\mathbf{x},t]\langle\boldsymbol{\xi}\rangle = \underline{e}\langle\boldsymbol{\xi}\rangle - \frac{\theta\,\|\boldsymbol{\xi}\|}{3} \,. \tag{15}$$

The peridynamic strain energy density at a point $\mathbf{x}$ of a linear elastic isotropic material is given as

$$\begin{aligned} W(\mathbf{x},t) &= \frac{k}{2}\theta^2 + \frac{\alpha}{2m} \int_{\mathcal{H}_\mathbf{x}} \underline{\omega}(\|\boldsymbol{\xi}\|) \left(\underline{e}^d\langle\boldsymbol{\xi}\rangle\right)^2 \mathrm{d}V_{\mathbf{x}'} \\ &= \frac{k}{2}\theta^2 + \frac{\alpha}{2m} (\underline{\omega}\,\underline{e}^d) \bullet \underline{e}^d \,, \end{aligned} \tag{16}$$

where k and α are the peridynamic constants that are determined by comparison with the CCM strain energy density in an infinite body under homogeneous deformation: $k = K$ and $\alpha = 15G$ in 3D, $k = K + G/9$ and $\alpha = 8G$ in 2D plane strain conditions, and $k = K + G(\nu+1)^2/(9(2\nu-1)^2)$ and $\alpha = 8G$ in 2D plane stress conditions [12,68], where K is the bulk modulus and G is the shear modulus. The bulk and shear moduli can be expressed in terms of the Young's modulus E and Poisson's ratio ν as $K = E/(3(1-2\nu))$ and $G = E/(2(1+\nu))$, respectively. Note that, by substituting Eq. (15) into Eq. (16), the peridynamic strain energy density can be rewritten as

$$\begin{aligned} W(\mathbf{x},t) &= \frac{k}{2}\theta^2 + \frac{\alpha}{2m} \int_{\mathcal{H}_\mathbf{x}} \underline{\omega}(\|\boldsymbol{\xi}\|) \left[\left(\underline{e}\langle\boldsymbol{\xi}\rangle\right)^2 - \frac{2}{3}\,\theta\,\|\boldsymbol{\xi}\|\,\underline{e}\langle\boldsymbol{\xi}\rangle + \frac{\theta^2\,\|\boldsymbol{\xi}\|^2}{9} \right] \mathrm{d}V_{\mathbf{x}'} \\ &= \frac{\alpha}{2m} \int_{\mathcal{H}_\mathbf{x}} \underline{\omega}(\|\boldsymbol{\xi}\|) \left(\underline{e}\langle\boldsymbol{\xi}\rangle\right)^2 \mathrm{d}V_{\mathbf{x}'} + \left(\frac{k}{2} - \frac{\alpha}{3c_\theta} + \frac{\alpha}{18}\right)\theta^2 \\ &= \frac{\alpha}{2m} (\underline{\omega}\,\underline{e}) \bullet \underline{e} + \left(\frac{k}{2} - \frac{\alpha}{3c_\theta} + \frac{\alpha}{18}\right)\theta^2 \,, \end{aligned} \tag{17}$$

where the first term is similar to the strain energy density in bond-based peridynamics, whereas the second term is characteristic of ordinary state-based peridynamics.

In ordinary state-based peridynamics [12], the force density vector state is aligned with the corresponding bond for any deformation, and its magnitude is obtained as the Fréchet derivative of the strain energy density with respect to the extension scalar state:

$$\underline{\mathbf{T}}[\mathbf{x},t]\langle\boldsymbol{\xi}\rangle = \frac{\underline{\omega}(\|\boldsymbol{\xi}\|)}{m} \left[\alpha\,\underline{e}\langle\boldsymbol{\xi}\rangle + c_\theta \left(k - \frac{2\alpha}{3c_\theta} + \frac{\alpha}{9}\right) \|\boldsymbol{\xi}\|\,\theta \right] \underline{\mathbf{M}}\langle\boldsymbol{\xi}\rangle \,, \tag{18}$$

Therefore, by substituting Eq. (18) into Eq. (7) and by taking into account that $\underline{e}\langle\boldsymbol{\xi}\rangle = \underline{e}\langle-\boldsymbol{\xi}\rangle$ and $\underline{\mathbf{M}}\langle\boldsymbol{\xi}\rangle = -\underline{\mathbf{M}}\langle-\boldsymbol{\xi}\rangle$, the bond force becomes

$$\mathbf{f}(\mathbf{x},\mathbf{x}',t) = \underline{\omega}(\|\boldsymbol{\xi}\|) \left[\alpha \left(\frac{1}{m(\mathbf{x})} + \frac{1}{m(\mathbf{x}')}\right) \underline{e}\langle\boldsymbol{\xi}\rangle + c_\theta \left(k - \frac{2\alpha}{3c_\theta} + \frac{\alpha}{9}\right) \|\boldsymbol{\xi}\| \left(\frac{\theta(\mathbf{x},t)}{m(\mathbf{x})} + \frac{\theta(\mathbf{x}',t)}{m(\mathbf{x}')}\right) \right] \underline{\mathbf{M}}\langle\boldsymbol{\xi}\rangle \,. \tag{19}$$

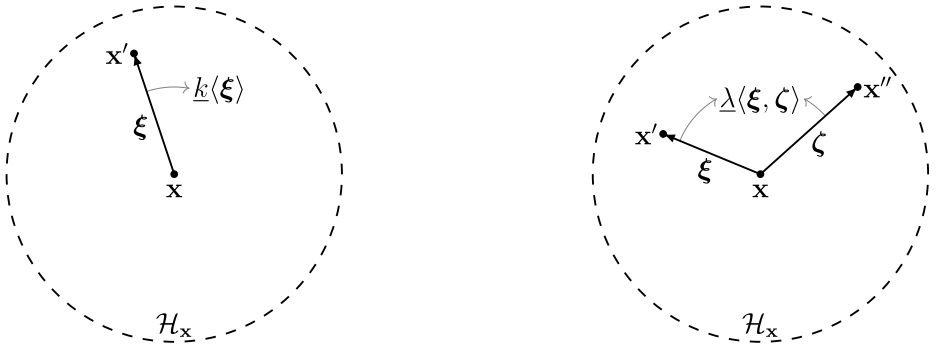

(a) *The single-bond micromodulus depends on the orientation of a single bond.*

(b) *The double-bond micromodulus depends on the orientations of a pair of bonds.*

Fig. 3. Micromoduli used in the new anisotropic peridynamic formulation.

Furthermore, if a body modeled with ordinary state-based peridynamics is subjected to a small homogeneous deformation for any time t, the coefficients $C_{ijk\ell}$ of the elasticity tensor are given from [66] as

$$C_{ijk\ell}(\mathbf{x}) = \frac{\alpha}{m}\int_{\mathcal{H}_{\mathbf{x}}} \underline{\omega}(\|\boldsymbol{\xi}\|)\frac{\xi_i\xi_j\xi_k\xi_\ell}{\|\boldsymbol{\xi}\|^2}\mathrm{d}V_{\mathbf{x}'} + \frac{c_\theta^2}{m^2}\left(k - \frac{2\alpha}{3c_\theta} + \frac{\alpha}{9}\right)\int_{\mathcal{H}_{\mathbf{x}}} \underline{\omega}(\|\boldsymbol{\xi}\|)\,\xi_i\xi_j\mathrm{d}V_{\mathbf{x}'}\int_{\mathcal{H}_{\mathbf{x}}} \underline{\omega}(\|\boldsymbol{\zeta}\|)\,\zeta_k\zeta_\ell\mathrm{d}V_{\mathbf{x}''}\,, \tag{20}$$

where $\boldsymbol{\xi} = \mathbf{x}' - \mathbf{x}$ and $\boldsymbol{\zeta} = \mathbf{x}'' - \mathbf{x}$ are two bonds in the neighborhood of point $\mathbf{x}$, and the subscripts denote the components of the bonds along i, j, k, or ℓ directions. These indices can be x or y in 2D, and x, y, or z in 3D. As in classical continuum mechanics, only two components of the elasticity tensor are independent from the others since the material is assumed to be isotropic.

Remark 1. It is worth noting that Eq. (20) is used to compute the PD elasticity tensor, which, in the case of non-homogeneous deformation, may be different from the CCM elasticity tensor (see, for example, [69]). However, assuming small homogeneous deformations within an entire neighborhood, the PD elasticity tensor coincide with the CCM one [66]. We consider this assumption in this and the following sections. In practice, where non-homogeneous deformations are present, the elasticity tensor is the same in PD and CCM in the limit of $\delta \to 0$ [70].

4. A new ordinary state-based formulation for anisotropic materials

Enhancing the peridynamic framework with the capability of modeling generally anisotropic materials is of paramount importance. For instance, advanced composite materials, frequently used in many engineering fields, such as aerospace, mechanical, civil, and many others, are anisotropic. We propose in the following an ordinary state-based formulation capable of handling any degree of material anisotropy.

To model the material anisotropy in ordinary state-based peridynamics, we introduce two distinct bond stiffness (scalar) functions, which are called *micromoduli* and denoted by $\underline{k}\langle\boldsymbol{\xi}\rangle$ and $\underline{\lambda}\langle\boldsymbol{\xi},\boldsymbol{\zeta}\rangle$. The former is named *single-bond micromodulus* because its value depends on the orientation of a single bond $\boldsymbol{\xi}$ (see Fig. 3(a)), whereas the latter is named *double-bond micromodulus* because its value depends on the orientations of a pair of bonds $\boldsymbol{\xi}$ and $\boldsymbol{\zeta}$ (see Fig. 3(b)). Note that, according to the definitions given in [12,66], $\underline{k}\langle\boldsymbol{\xi}\rangle$ is a scalar-valued state and $\underline{\lambda}\langle\boldsymbol{\xi},\boldsymbol{\zeta}\rangle$ is a scalar-valued double state. These micromoduli have the same units of measurements as the components of the CCM elasticity tensor, i.e., a force per unit area. The micromoduli $\underline{k}\langle\boldsymbol{\xi}\rangle$ and $\underline{\lambda}\langle\boldsymbol{\xi},\boldsymbol{\zeta}\rangle$ will be defined for the 2D and 3D cases in the following sections. In particular, to satisfy the major symmetry of the elasticity tensor in the peridynamic anisotropic model, $\underline{\lambda}$ must have the following property (see Appendix A): $\underline{\lambda}\langle\boldsymbol{\xi},\boldsymbol{\zeta}\rangle = \underline{\lambda}\langle\boldsymbol{\zeta},\boldsymbol{\xi}\rangle$.

For brevity of notation, we also introduce a new scalar quantity, named the *microforce*, at a point $\mathbf{x}$ that depends on the bond $\boldsymbol{\xi}$:

$$\begin{aligned}\Lambda(\boldsymbol{\xi},\mathbf{x},t) &= \frac{1}{m}\int_{\mathcal{H}_{\mathbf{x}}} \underline{\lambda}\langle\boldsymbol{\xi},\boldsymbol{\zeta}\rangle\,\underline{\omega}(\|\boldsymbol{\zeta}\|)\,\|\boldsymbol{\zeta}\|\,\underline{e}\langle\boldsymbol{\zeta}\rangle\mathrm{d}V_{\mathbf{x}''}\\ &= \frac{1}{m}\,\underline{\lambda}\bullet(\underline{\omega}\,\underline{x}\,\underline{e})\,.\end{aligned} \tag{21}$$

Where possible, we will omit the dependence on position $\mathbf{x}$ and on time t: $\Lambda(\boldsymbol{\xi}) = \Lambda(\boldsymbol{\xi},\mathbf{x},t)$. As shown in Fig. 3(b), the double-bond micromodulus depends on a pair of bonds, i.e., $\boldsymbol{\xi}$ and $\boldsymbol{\zeta}$, both associated to the same point $\mathbf{x}$. On the other hand, the microforce explicitly depends on a single bond $\boldsymbol{\xi}$, since the contribution of the bond $\boldsymbol{\zeta}$ is integrated over the neighborhood of point $\mathbf{x}$. The microforce embeds information about the deformation state of the whole neighborhood of point $\mathbf{x}$, similarly to the dilatation defined in the ordinary state-based peridynamic formulation for isotropic materials (see Eq. (14)). Nonetheless, the microforce also contains information about the stiffness of the bonds within the neighborhood (through the double-bond micromodulus), which is not true

for the dilatation. The microforce has the same units of measurements as the double-bond micromodulus, i.e., a force per unit area. This is the reason why the quantity computed in Eq. (21) is named *microforce*.

The strain energy density is reformulated such that the stiffness coefficients of the bonds depend on their orientations:

$$\begin{aligned} W(\mathbf{x},t) &= \frac{1}{2m}\int_{\mathcal{H}_\mathbf{x}} \underline{k}\langle\xi\rangle\,\underline{\omega}(\|\xi\|)\left(\underline{e}\langle\xi\rangle\right)^2 \mathrm{d}V_{\mathbf{x}'} + \frac{1}{2m}\int_{\mathcal{H}_\mathbf{x}} \underline{\omega}(\|\xi\|)\,\|\xi\|\,\underline{e}\langle\xi\rangle\,\Lambda(\xi)\mathrm{d}V_{\mathbf{x}'} \\ &= \frac{1}{2m}(\underline{k}\,\underline{\omega}\,\underline{e})\bullet\underline{e} + \frac{1}{2m^2}(\underline{\omega}\,\underline{x}\,\underline{e})\bullet\underline{\lambda}\bullet(\underline{\omega}\,\underline{x}\,\underline{e})\,. \end{aligned} \tag{22}$$

The first and second terms of the strain energy density depend on the single-bond and double-bond micromoduli, respectively. The difference between the strain energy density for isotropic and anisotropic materials lies only in the bond stiffness functions: for isotropic materials the stiffness functions are constant and can be pulled out from the integrals (see Eq. (17)), whereas for anisotropic materials the stiffness functions, i.e., the micromoduli, depend on bond orientations and must be kept inside the integrals (see Eq. (22)).

Therefore, the force density vector state, whose magnitude is the Fréchet derivative of W with respect to $\underline{e}$ (see Appendix A for details), is given as

$$\underline{\mathbf{T}}[\mathbf{x},t]\langle\xi\rangle = \frac{\underline{\omega}(\|\xi\|)}{m}\left[\underline{k}\langle\xi\rangle\,\underline{e}\langle\xi\rangle + \|\xi\|\,\Lambda(\xi)\right]\underline{\mathbf{M}}\langle\xi\rangle\,. \tag{23}$$

Note that the first term depends on a single bond (as in bond-based peridynamics), whereas the second term substitutes the term containing the dilatation in ordinary state-based peridynamics for isotropic materials. The force of any bond in the new formulation is obtained by substituting Eq. (23) into Eq. (7):

$$\mathbf{f}(\mathbf{x},\mathbf{x}',t) = \underline{\omega}(\|\xi\|)\left[\left(\frac{1}{m(\mathbf{x})}+\frac{1}{m(\mathbf{x}')}\right)\underline{k}\langle\xi\rangle\,\underline{e}\langle\xi\rangle + \left(\frac{\Lambda(\xi,\mathbf{x},t)}{m(\mathbf{x})}+\frac{\Lambda(\xi,\mathbf{x}',t)}{m(\mathbf{x}')}\right)\|\xi\|\right]\underline{\mathbf{M}}\langle\xi\rangle\,, \tag{24}$$

where $\underline{e}\langle\xi\rangle = \underline{e}\langle-\xi\rangle$, $\underline{\mathbf{M}}\langle\xi\rangle = -\underline{\mathbf{M}}\langle-\xi\rangle$, $\underline{k}\langle\xi\rangle = \underline{k}\langle-\xi\rangle$ (see definitions of the single-bond stiffness function in Eq. (28) in 2D and in Eq. (32) in 3D), and $\Lambda(\xi,\mathbf{x},t) = \Lambda(-\xi,\mathbf{x},t)$ since $\underline{\lambda}\langle\xi,\zeta\rangle = \underline{\lambda}\langle-\xi,\zeta\rangle$ (see definitions of the double-bond stiffness function in Eq. (29) in 2D and in Eq. (33) in 3D).

In the linearized state-based peridynamic theory [66], the material response is described by the *modulus state*, that can be obtained as the second Fréchet derivative of the strain energy density. In the present formulation for anisotropic materials, the modulus (double) state is given from Appendix A as

$$\underline{\mathbb{K}}\langle\xi,\zeta\rangle = \frac{\underline{\omega}(\|\xi\|)}{m}\left[\underline{k}\langle\xi\rangle\,\frac{\Delta(\zeta-\xi)}{\|\xi\|\,\|\zeta\|} + \frac{1}{m}\,\underline{\lambda}\langle\xi,\zeta\rangle\,\underline{\omega}(\|\zeta\|)\right]\xi\otimes\zeta\,, \tag{25}$$

where Δ is the Dirac delta function and $\otimes$ indicates a dyadic product. This means that any of the results in [66] are valid for the proposed formulation without further proofs. As a result, the coefficients of the elasticity tensor in an anisotropic material are derived as

$$C_{ijk\ell}(\mathbf{x}) = \frac{1}{m}\int_{\mathcal{H}_\mathbf{x}} \underline{k}\langle\xi\rangle\,\underline{\omega}(\|\xi\|)\frac{\xi_i\xi_j\xi_k\xi_\ell}{\|\xi\|^2}\mathrm{d}V_{\mathbf{x}'} + \frac{1}{m^2}\int_{\mathcal{H}_\mathbf{x}}\int_{\mathcal{H}_\mathbf{x}} \underline{\lambda}\langle\xi,\zeta\rangle\,\underline{\omega}(\|\xi\|)\,\underline{\omega}(\|\zeta\|)\,\xi_i\xi_j\zeta_k\zeta_\ell\mathrm{d}V_{\mathbf{x}''}\mathrm{d}V_{\mathbf{x}'}\,. \tag{26}$$

Remark 1 applies also to Eq. (26). As it can be seen by comparing Eqs. (20) and (26), the only difference with the peridynamic model for isotropic materials is that, for anisotropic materials, the bond stiffness functions, i.e., the micromoduli, are inside the integrals because they depend on the bond direction.

Notably, the PD elasticity tensor computed with Eq. (26) exhibit the major and minor symmetries, i.e., $C_{ijk\ell} = C_{k\ell ij}$ and $C_{ijk\ell} = C_{jik\ell} = C_{ij\ell k}$, as in classical continuum mechanics (see Section 2). It is clear that the order of the indices in the first term in the right-hand side of Eq. (26), which is similar to the bond-based peridynamic term, is irrelevant. This is the reason why the bond-based formulation must satisfy the Cauchy's relations ($C_{ijk\ell} = C_{ikj\ell}$) [45]. Hence, there is the need of the additional term to model fully anisotropic materials not following Cauchy's relations, as it was done in ordinary state-based peridynamics to model the Poisson's effect in isotropic materials [12] (see Section 3). In fact, the second term in the right-hand side of Eq. (26) does *not* necessarily satisfy the Cauchy's relations.

4.1. 2D micromoduli

In CCM, the elasticity tensor for 2D fully anisotropic materials has 6 independent components due to the major and minor symmetries:

$$\begin{bmatrix}\sigma_{xx}\\ \sigma_{yy}\\ \sigma_{xy}\end{bmatrix} = \begin{bmatrix}C_{xxxx} & C_{xxyy} & C_{xxxy}\\ \cdot & C_{yyyy} & C_{yyxy}\\ \cdot & \cdot & C_{xyxy}\end{bmatrix}\begin{bmatrix}\varepsilon_{xx}\\ \varepsilon_{yy}\\ 2\varepsilon_{xy}\end{bmatrix}, \tag{27}$$

where Voigt notation was used. Furthermore, in 2D there is one Cauchy's relation, i.e., $C_{xyxy} = C_{xxyy}$.

The choice of the bond stiffness functions is not univocal. These functions should be chosen so that the number of their constants matches the number of independent components of the elasticity tensor, namely 6 in 2D. Inspired by [45], we define the single-bond micromodulus as a 4th-order polynomial of the bond direction components:

$$\underline{k}\langle\boldsymbol{\xi}\rangle = \frac{1}{\|\xi\|^4}\left(k_{xxxx}\,\xi_x^4 + k_{xxxy}\,\xi_x^3\xi_y + k_{xxyy}\,\xi_x^2\xi_y^2 + k_{yyxy}\,\xi_x\xi_y^3 + k_{yyyy}\,\xi_y^4\right), \tag{28}$$

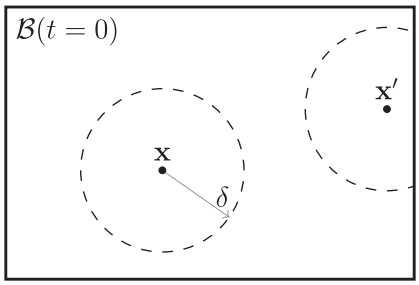

Fig. 4. Point $\mathbf{x}$ in the bulk of the body has a complete neighborhood, whereas point $\mathbf{x}'$ close to the boundary has an incomplete neighborhood.

where the constants will be determined by equalizing the components of the CCM elasticity tensor with those obtained with peridynamics in Eq. (26). It is worth noting that there are 5 unknown constants in Eq. (28), but 6 independent components of the CCM elasticity tensor. In fact, the sixth constant (that would have been k_{xyxy}) cannot be modeled with the single-bond micromodulus due to the Cauchy's relation. Therefore, we define the double-bond micromodulus $\underline{\lambda}$ to "release" the last constant λ_{xyxy} from the above-mentioned restriction:

$$\underline{\lambda}\langle\boldsymbol{\xi},\boldsymbol{\zeta}\rangle = \frac{1}{\|\boldsymbol{\xi}\|^2\|\boldsymbol{\zeta}\|^2}\,\lambda_{xyxy}\,\xi_x\xi_y\zeta_x\zeta_y\,. \tag{29}$$

Note that $\underline{\lambda}\langle\boldsymbol{\xi},\boldsymbol{\zeta}\rangle = \underline{\lambda}\langle\boldsymbol{\zeta},\boldsymbol{\xi}\rangle$ to retain the major symmetry of the PD elasticity tensor (see Appendix A).

Therefore, we use Eq. (26) for a peridynamic point with a complete neighborhood to write 6 equations corresponding to the 6 independent components of the CCM elasticity tensor. The unknowns of this system of equations are the 6 constants appearing in the micromoduli in Eqs. (28) and (29), as shown in Appendix B. Therefore, by solving these equations, one can determine the unknown constants as functions of the components of the CCM elasticity tensor as

$$k_{xxxx} = 5C_{xxxx} - 10C_{xxyy} + C_{yyyy}\,, \tag{30a}$$
$$k_{xxxy} = 40C_{xxxy} - 24C_{yyxy}\,, \tag{30b}$$
$$k_{xxyy} = 76C_{xxyy} - 10C_{xxxx} - 10C_{yyyy}\,, \tag{30c}$$
$$k_{yyxy} = 40C_{yyxy} - 24C_{xxxy}\,, \tag{30d}$$
$$k_{yyyy} = 5C_{yyyy} - 10C_{xxyy} + C_{xxxx}\,, \tag{30e}$$
$$\lambda_{xyxy} = 64C_{xyxy} - 64C_{xxyy}\,. \tag{30f}$$

These bond stiffness constants are then used in Eqs. (28) and (29) to ultimately define the micromoduli in the 2D anisotropic peridynamic model.

Remark 2. The proposed peridynamic formulation is able to model, in general, anisotropic materials. Since isotropic materials are a special case of anisotropic ones, they also can be modeled with the proposed formulation. In 2D classical continuum mechanics, isotropic materials are characterized by $C_{yyyy} = C_{xxxx}$, $C_{xyxy} = (C_{xxxx} - C_{xxyy})/2$, $C_{xxxy} = C_{yyxy} = 0$, where C_{xxxx} and C_{xxyy} are the only components of the elasticity tensor that are independent from the others. It is worth noting that, differently from the ordinary state-based formulation in [12] (see Section 3), the micromoduli $\underline{k}$ and $\underline{\lambda}$ may still depend on the bond orientation to model isotropic materials. Nonetheless, the macroscopic stiffness properties of the proposed model exhibit an isotropic behavior, as shown in Fig. 8 in Section 6.1.

Remark 3. Note that some constants of the micromoduli, computed with Eq. (30), may be negative. However, the macroscopic stiffness properties are correctly reproduced in any case because Eq. (26) was used to determine the micromoduli. Positive micromoduli is a sufficient, but not necessary, condition for the peridynamic constitutive model to be numerically stable [43,71]. The possible presence of negative micromoduli, and its consequences on the numerical results, will be further investigated in the future.

Remark 4. Since the constants of the micromoduli are determined for a peridynamic point with a complete neighborhood, the points close to the boundaries of the body (with an incomplete neighborhood, as shown in Fig. 4) exhibit an undesired stiffness variation. This phenomenon, called *surface effect*, is well-known in peridynamics [72–74], and is the cause of differences between PD and CCM solutions close to the boundaries of the body. The stiffness variation due to the surface effect can be reduced by decreasing the value of the horizon size δ.

4.2. 3D micromoduli

The elasticity tensor for a 3D fully anisotropic material is expressed by means of Voigt notation as

$$\begin{bmatrix}\sigma_{xx}\\ \sigma_{yy}\\ \sigma_{zz}\\ \sigma_{yz}\\ \sigma_{xz}\\ \sigma_{xy}\end{bmatrix} = \begin{bmatrix}C_{xxxx} & C_{xxyy} & C_{xxzz} & C_{xxyz} & C_{xxxz} & C_{xxxy}\\ \cdot & C_{yyyy} & C_{yyzz} & C_{yyyz} & C_{yyxz} & C_{yyxy}\\ \cdot & \cdot & C_{zzzz} & C_{zzyz} & C_{zzxz} & C_{zzxy}\\ \cdot & \cdot & \cdot & C_{yzyz} & C_{yzxz} & C_{yzxy}\\ \cdot & \cdot & \cdot & \cdot & C_{xzxz} & C_{xzxy}\\ \cdot & \cdot & \cdot & \cdot & \cdot & C_{xyxy}\end{bmatrix}\begin{bmatrix}\varepsilon_{xx}\\ \varepsilon_{yy}\\ \varepsilon_{zz}\\ 2\varepsilon_{xy}\\ 2\varepsilon_{xz}\\ 2\varepsilon_{xy}\end{bmatrix}, \tag{31}$$

where the 21 independent components are highlighted. Furthermore, there are 6 Cauchy's relations in 3D: $C_{yzyz} = C_{yyzz}$, $C_{xzxz} = C_{xxzz}$, $C_{xyxy} = C_{xxyy}$, $C_{yzxz} = C_{zzxy}$, $C_{yzxy} = C_{yyxz}$, $C_{xzxy} = C_{xxyz}$.

The choice of the bond stiffness functions is not univocal. These functions should be chosen so that the number of their constants matches the number of independent components of the elasticity tensor, namely 21 in 3D. Inspired by [45], we define the single-bond micromodulus as a 4th-order polynomial of the bond direction components:

$$\begin{aligned}\underline{k}\langle\boldsymbol{\xi}\rangle = \frac{1}{\|\boldsymbol{\xi}\|^4}\Big(&k_{xxxx}\,\xi_x^4 + k_{xxxy}\,\xi_x^3\xi_y + k_{xxxz}\,\xi_x^3\xi_z + k_{xxyy}\,\xi_x^2\xi_y^2 + k_{xxyz}\,\xi_x^2\xi_y\xi_z + k_{xxzz}\,\xi_x^2\xi_z^2 + k_{yyxy}\,\xi_x\xi_y^3\\ &+k_{yyxz}\,\xi_x\xi_y^2\xi_z + k_{zzxy}\,\xi_x\xi_y\xi_z^2 + k_{zzxz}\,\xi_x\xi_z^3 + k_{yyyy}\,\xi_y^4 + k_{yyyz}\,\xi_y^3\xi_z + k_{yyzz}\,\xi_y^2\xi_z^2 + k_{zzyz}\,\xi_y\xi_z^3 + k_{zzzz}\,\xi_z^4\Big),\end{aligned} \tag{32}$$

where there are 15 single-bond stiffness constants to be determined. Similarly to the proposed 2D model, the double-bond micromodulus $\underline{\lambda}$ is defined to correctly reproduce the components of the elasticity tensor that are restrained in the single-bond micromodulus by the Cauchy's relations:

$$\begin{aligned}\underline{\lambda}\langle\boldsymbol{\xi},\boldsymbol{\zeta}\rangle = \frac{1}{\|\boldsymbol{\xi}\|^2\|\boldsymbol{\zeta}\|^2}\Big[&\lambda_{yzyz}\,\xi_y\xi_z\zeta_y\zeta_z + \lambda_{xzxz}\,\xi_x\xi_z\zeta_x\zeta_z + \lambda_{xyxy}\,\xi_x\xi_y\zeta_x\zeta_y + \frac{\lambda_{yzxz}}{2}\left(\xi_y\xi_z\zeta_x\zeta_z + \xi_x\xi_z\zeta_y\zeta_z\right)\\ &+\frac{\lambda_{yzxy}}{2}\left(\xi_y\xi_z\zeta_x\zeta_y + \xi_x\xi_y\zeta_y\zeta_z\right) + \frac{\lambda_{xzxy}}{2}\left(\xi_x\xi_z\zeta_x\zeta_y + \xi_x\xi_y\zeta_x\zeta_z\right)\Big].\end{aligned} \tag{33}$$

Note that the double-bond micromodulus is defined such as $\underline{\lambda}\langle\boldsymbol{\xi},\boldsymbol{\zeta}\rangle = \underline{\lambda}\langle\boldsymbol{\zeta},\boldsymbol{\xi}\rangle$ to retain the major symmetry of the PD elasticity tensor (see Appendix A).

Appendix C shows how to write 21 equations with Eq. (26) corresponding to the independent components of the CCM elasticity tensor and to solve for the 21 bond stiffness constants in Eq. (32) and (33):

$$k_{xxxx} = 15C_{xxxx} + \frac{15}{8}\left(C_{yyyy} + C_{zzzz}\right) - \frac{45}{2}\left(C_{xxyy} + C_{xxzz}\right) + \frac{15}{4}C_{yyzz}, \tag{34a}$$

$$k_{yyyy} = 15C_{yyyy} + \frac{15}{8}\left(C_{xxxx} + C_{zzzz}\right) - \frac{45}{2}\left(C_{xxyy} + C_{yyzz}\right) + \frac{15}{4}C_{xxzz}, \tag{34b}$$

$$k_{zzzz} = 15C_{zzzz} + \frac{15}{8}\left(C_{xxxx} + C_{yyyy}\right) - \frac{45}{2}\left(C_{xxzz} + C_{yyzz}\right) + \frac{15}{4}C_{xxyy}, \tag{34c}$$

$$k_{xxyy} = \frac{765}{4}C_{xxyy} - \frac{75}{4}\left(C_{xxzz} + C_{yyzz}\right) - \frac{45}{2}\left(C_{xxxx} + C_{yyyy}\right) + \frac{15}{4}C_{zzzz}, \tag{34d}$$

$$k_{xxzz} = \frac{765}{4}C_{xxzz} - \frac{75}{4}\left(C_{xxyy} + C_{yyzz}\right) - \frac{45}{2}\left(C_{xxxx} + C_{zzzz}\right) + \frac{15}{4}C_{yyyy}, \tag{34e}$$

$$k_{yyzz} = \frac{765}{4}C_{yyzz} - \frac{75}{4}\left(C_{xxyy} + C_{xxzz}\right) - \frac{45}{2}\left(C_{yyyy} + C_{zzzz}\right) + \frac{15}{4}C_{xxxx}, \tag{34f}$$

$$k_{xxxy} = 105C_{xxxy} - \frac{105}{2}\left(C_{yyxy} + C_{zzxy}\right), \tag{34g}$$

$$k_{yyxy} = 105C_{yyxy} - \frac{105}{2}\left(C_{xxxy} + C_{zzxy}\right), \tag{34h}$$

$$k_{zzxy} = 420C_{zzxy} - \frac{105}{2}\left(C_{xxxy} + C_{yyxy}\right), \tag{34i}$$

$$k_{xxxz} = 105C_{xxxz} - \frac{105}{2}\left(C_{yyxz} + C_{zzxz}\right), \tag{34j}$$

$$k_{yyxz} = 420C_{yyxz} - \frac{105}{2}\left(C_{xxxz} + C_{zzxz}\right), \tag{34k}$$

$$k_{zzxz} = 105C_{zzxz} - \frac{105}{2}\left(C_{xxxz} + C_{yyxz}\right), \tag{34l}$$

$$k_{xxyz} = 420C_{xxyz} - \frac{105}{2}\left(C_{yyyz} + C_{zzyz}\right), \tag{34m}$$

$$k_{yyyz} = 105C_{yyyz} - \frac{105}{2}\left(C_{xxyz} + C_{zzyz}\right), \tag{34n}$$

$$k_{zzyz} = 105C_{zzyz} - \frac{105}{2}\left(C_{xxyz} + C_{yyyz}\right), \tag{34o}$$

$$\lambda_{xyxy} = 225\left(C_{xyxy} - C_{xxyy}\right), \tag{34p}$$

$$\lambda_{xzxz} = 225\left(C_{xzxz} - C_{xxzz}\right), \tag{34q}$$

$$\lambda_{yzyz} = 225\left(C_{yzyz} - C_{yyzz}\right), \tag{34r}$$

$$\lambda_{yzxz} = 450\left(C_{yzxz} - C_{zzxy}\right), \tag{34s}$$

$$\lambda_{yzxy} = 450\left(C_{yzxy} - C_{yyxz}\right), \tag{34t}$$

$$\lambda_{xzxy} = 450\left(C_{xzxy} - C_{xxyz}\right). \tag{34u}$$

Note that Remarks 2, 3, and 4 are valid also in the 3D case.

4.3. Comparison with other peridynamic formulations for anisotropic materials

Most of the peridynamic literature has treated materials with isotropic properties, but some formulations and numerical methods have been developed to model anisotropic materials. Among these approaches, most have been applied within the framework of bond-based peridynamics, due to the simplicity of the formulation, or non-ordinary state-based peridynamics, thanks to the possibility of incorporating any constitutive law of classical continuum mechanics.

In order to model uni-directional fiber-reinforced composites, the authors of [34] proposed to distinguish in the bond-based formulation between two types of bonds, i.e., the fiber bonds (parallel to the fiber direction) and matrix bonds (in all other directions). Each bond stiffness is fitted to the bulk elastic modulus of the corresponding type. This approach is used to model with the meshfree method the composite plies with 2D nodal grids, but it can be extended to 3D laminates by adding interlaminar bonds between the plies. Several works [35–37] followed this type of approach to model composite materials. A similar method was also used to model polycrystalline materials [39]. Since the classical mechanical theory assumes a continuous variation of the mechanical properties with the orientation of the fibers, the authors of [38,41–44] proposed continuous functions to describe the dependency of the bond stiffness with respect to its orientation. The problem of determining the stiffness of the bonds in the discretized model for bond-based peridynamics to reproduce the anisotropic properties of a medium, can also be solved by means of the least-square method [46]. All these models allowed to obtain numerical results of fracture phenomena in good agreement with experimental observations. However, in bond-based peridynamics the bond force is defined by a pair potential function, which implies that the components of the elasticity tensor must satisfy the Cauchy's relations [45,65]. This means that bond-based peridynamics is not suitable to model fully anisotropic media because some of the elastic coefficients have a fixed value. Since the model in this work is set in the context of ordinary state-based peridynamics, it is not affected by these limitations.

To overcome the restrictions given by Cauchy's relations, the bond-based formulation can be extended to include shear deformability of the bonds [50–54]. However, to avoid an incorrect description of the mechanical behavior of bodies under non-homogeneous deformation, these models should introduce the rotational degrees of freedom for the peridynamic points [51]. These models have been shown to provide the possibility of modeling 2D orthotropic materials without the restrictions given by the Cauchy's relations. Nonetheless, a 3D model including bond shear deformability would require a doubling of the number of the degrees of freedom for each node with respect to a 2D model (from 3 to 6), notably increasing the computational cost of the simulation. The proposed model for anisotropic materials relies only on translational degrees of freedom for the peridynamic points, and does not consider rotational degrees of freedom.

Another approach to model the mechanical properties of materials without the restrictions of the Cauchy's relations is to use multi-body potentials. Using this approach, a recent theory, called *continuum-kinematics-inspired peridynamics* [47,48], reformulates the interactions between points such that the nonlocal kinematics coincide with that of classical continuum kinematics. This formulation was generalized for 2D orthotropic and 3D transversely isotropic materials [49], but some values of the elastic coefficients are fixed a priori. Conversely, all the elastic coefficients can be correctly reproduced by the proposed model (see Sections 6.1 and 6.2).

In the literature, the most commonly used approach to overcome the limitations of bond-based peridynamics is to adopt the state-based version of the theory [12]. This theory makes use of pointwise deformation measures that allow for the mechanical properties to be independent from the Cauchy's relations. Ordinary state-based peridynamics was used to model 2D orthotropic media by introducing two additional bond stiffness coefficients along the two principal axes of the material [56]. However, the off-axis stiffness exhibits considerable differences with respect to that predicted by classical continuum mechanics. Furthermore, it is not clear if this method can be generalized to 3D models. The ordinary state-based model proposed in this work overcomes these limitations, since it allows to accurately reproduce any component of the CCM elasticity tensor both in 2D and 3D cases (see Sections 6.1 and 6.2).

Non-ordinary state-based peridynamics is a generalization of the ordinary version. Since this formulation uses a classical stress tensor to compute the force state, it allows to directly incorporate the constitutive laws of classical continuum mechanics within the peridynamic framework. This approach is often called *correspondence model*. The correspondence model that allows to reproduce all the components of the CCM elasticity tensor for a fully anisotropic material was developed in [58] for the 2D case and in [61] for the 3D case. Several other correspondence models in the framework of non-ordinary state-based peridynamics were developed to simulate phenomena that included an anisotropic material behavior, such as the plastic deformation and fracture of unidirectional laminates [57], the fluid-driven fracturing in orthotropic poroelastic media [59], and the anisotropic plasticity of sheet metals [60]. However, non-ordinary state-based peridynamic models suffer from instability issues, such as zero-energy modes. Therefore, they require additional stabilization techniques to obtain reasonable numerical results [62–64]. On the other hand, the model proposed in this work does not require any stabilization method.

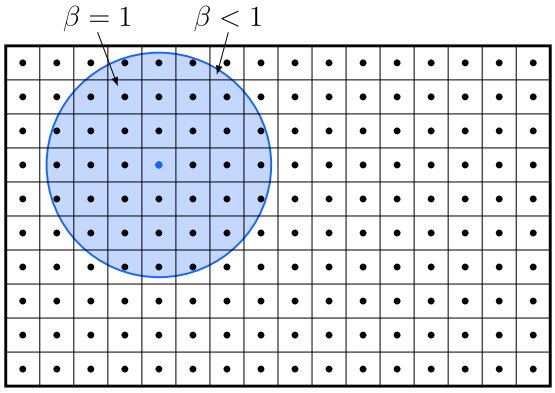

Fig. 5. Discretization of a body modeled with peridynamics ($\overline{m} = \delta/\Delta x = 3.3$) by means of the meshfree method with a uniform grid spacing. The neighborhood of a node is highlighted in blue and the quadrature coefficients (fraction of nodal volume that lies within the neighborhood) of two nodes are shown.

5. Numerical implementation

We adopt here the so-called *meshfree method* to discretize the peridynamic equations [75]. To reduce the computational cost, the coupling with CCM-based methods [76–79], the Fast Convolution-Based Method (FCBM) [80,81], or the hybrid method developed in [82,83] can be used, but this is not pursued in this work. In the meshfree method, the body is often discretized with a regular grid of nodes, as shown in Fig. 5. Each node represents a finite volume of Δx^3 in 3D and $t\Delta x^2$ in 2D, where Δx is the uniform grid spacing and t is the thickness of the body.

The spatial integration of the peridynamic integral operator is carried out by transforming the integral over the neighborhood into a summation of integrals over nodal volumes, to which the midpoint quadrature rule is then applied [75]. Thus, the peridynamic equation of motion, discretized from Eq. (5), at a time $t \geq 0$ at a node $\mathbf{x}_p$ is given as

$$\rho(\mathbf{x}_p)\,\ddot{\mathbf{u}}(\mathbf{x}_p,t) = \sum_{q\in\mathcal{H}_p} \mathbf{f}(\mathbf{x}_p,\mathbf{x}_q,t)\,\beta_{pq}\,\Delta V + \mathbf{b}(\mathbf{x}_p,t)\,, \tag{35}$$

where ρ is the density of the material, $\ddot{\mathbf{u}}$ is the acceleration field, $\mathcal{H}_p$ is the neighborhood of node $\mathbf{x}_p$, $\mathbf{f}$ is the bond force (force per unit volume squared), β_{pq} is the quadrature coefficient associated with the bond between nodes $\mathbf{x}_p$ and $\mathbf{x}_q$, and $\mathbf{b}$ is the external force density field. Under static conditions, the peridynamic equilibrium equation in the discretized model is given as

$$-\sum_{q\in\mathcal{H}_p} \mathbf{f}(\mathbf{x}_p,\mathbf{x}_q)\,\beta_{pq}\,\Delta V = \mathbf{b}(\mathbf{x}_p)\,. \tag{36}$$

The quadrature coefficient β is introduced because the contribution of each node should be proportional to the fraction of its volume that actually lies within the neighborhood [84–86]. Hence, $\beta_{pq} = 1$ for nodes $\mathbf{x}_q$ that have the whole volume inside the neighborhood $\mathcal{H}_p$ and $0 < \beta_{pq} < 1$ for those that have only a portion of volume inside $\mathcal{H}_q$ (see Fig. 5). In this work, we adopt the method developed in [86] for the computation of β.

The extension scalar state and the direction vector state are numerically evaluated, respectively, as

$$\underline{e}_{pq} = \|\boldsymbol{\xi}_{pq} + \mathbf{u}(\mathbf{x}_q,t) - \mathbf{u}(\mathbf{x}_p,t)\| - \|\boldsymbol{\xi}_{pq}\|\,, \tag{37}$$

$$\underline{\mathbf{M}}_{pq} = \frac{\boldsymbol{\xi}_{pq} + \mathbf{u}(\mathbf{x}_q,t) - \mathbf{u}(\mathbf{x}_p,t)}{\|\boldsymbol{\xi}_{pq} + \mathbf{u}(\mathbf{x}_q,t) - \mathbf{u}(\mathbf{x}_p,t)\|}\,, \tag{38}$$

where the bond between the nodes $\mathbf{x}_p$ and $\mathbf{x}_q$ is $\boldsymbol{\xi}_{pq} = \mathbf{x}_q - \mathbf{x}_p$ and $\mathbf{u}$ is the displacement field. Under the assumption of small displacements, these quantities can be simplified as $\underline{\mathbf{M}}_{pq} = \boldsymbol{\xi}_{pq}/\|\boldsymbol{\xi}_{pq}\|$ and $\underline{e}_{pq} = [\mathbf{u}(\mathbf{x}_q,t) - \mathbf{u}(\mathbf{x}_p,t)] \cdot \underline{\mathbf{M}}_{pq}$. The weighted volume $m_p = m(\mathbf{x}_p)$ is computed in the discretized PD model as

$$m_p = \sum_{q\in\mathcal{H}_p} \underline{\omega}(\|\boldsymbol{\xi}_{pq}\|)\,\|\boldsymbol{\xi}_{pq}\|^2\,\beta_{pq}\,\Delta V\,, \tag{39}$$

where the adopted influence function is $\underline{\omega}(\|\boldsymbol{\xi}_{pq}\|) = \exp(-\|\boldsymbol{\xi}_{pq}\|^2/\delta^2)$. Similarly, the microforce is evaluated as

$$\Lambda(\boldsymbol{\xi}_{pq},\mathbf{x}_p,t) = \frac{1}{m_p}\sum_{r\in\mathcal{H}_p} \underline{\lambda}\langle\boldsymbol{\xi}_{pq},\boldsymbol{\zeta}_{pr}\rangle\,\underline{\omega}(\|\boldsymbol{\zeta}_{pr}\|)\,\|\boldsymbol{\zeta}_{pr}\|\,\underline{e}_{pr}\,\beta_{pr}\,\Delta V\,, \tag{40}$$

where $\boldsymbol{\zeta}_{pr} = \mathbf{x}_r - \mathbf{x}_p$. Therefore, the force in a bond $\boldsymbol{\xi}_{pq}$ for the new ordinary state-based peridynamic formulation for anisotropic materials is given as

$$\mathbf{f}(\mathbf{x}_p,\mathbf{x}_q,t) = \underline{\omega}(\|\boldsymbol{\xi}_{pq}\|)\left[\left(\frac{1}{m_p}+\frac{1}{m_q}\right)\underline{k}\langle\boldsymbol{\xi}_{pq}\rangle\,\underline{e}_{pq} + \left(\frac{\Lambda(\boldsymbol{\xi}_{pq},\mathbf{x}_p,t)}{m_p} + \frac{\Lambda(\boldsymbol{\xi}_{pq},\mathbf{x}_q,t)}{m_q}\right)\|\boldsymbol{\xi}_{pq}\|\right]\underline{\mathbf{M}}_{pq}\,. \tag{41}$$

Table 1
Properties of an orthotropic material (graphite fabric-carbon matrix composite material) and an isotropic material (steel) [5].

Material	Elastic moduli	Shear moduli	Poisson's ratios
Composite material	$E_1 = 173.06\,\text{GPa}$	$G_{12} = 9.38\,\text{GPa}$	$\nu_{12} = 0.036$
	$E_2 = 33.09\,\text{GPa}$	$G_{13} = 8.27\,\text{GPa}$	$\nu_{13} = 0.25$
	$E_3 = 5.17\,\text{GPa}$	$G_{23} = 3.24\,\text{GPa}$	$\nu_{23} = 0.171$
Steel	$E = 206.84\,\text{GPa}$	$G = 80.17\,\text{GPa}$	$\nu = 0.29$

For static problems, a linear system of equations can be obtained by substituting Eq. (41) into Eq. (36). Dirichlet boundary conditions are imposed over a fictitious layer of thickness δ, whereas Neumann boundary conditions are distributed over a layer of thickness δ within the region of the body closest to the boundary [87]. For simplicity, more accurate methods to impose peridynamic boundary conditions, such as the mirror node method [88] and the surface node method [89], are not used in this work. We iteratively solve the system of equations by means of the conjugate gradient method [90]. The relative tolerance for convergence is chosen as 10^{-6} in 2D models and, to reduce the computational cost, as 10^{-4} in 3D models.

The components of the elasticity tensor in an anisotropic material are evaluated in the discretized model as

$$C_{ijk\ell}(\mathbf{x}_p) = \frac{1}{m_p} \sum_{q \in \mathcal{H}_p} \underline{k}\langle \boldsymbol{\xi}_{pq} \rangle \, \underline{\omega}(\|\boldsymbol{\xi}_{pq}\|) \, \frac{\xi_i \xi_j \xi_k \xi_\ell}{\|\boldsymbol{\xi}_{pq}\|^2} \, \beta_{pq} \, \Delta V + \frac{1}{m_p^2} \sum_{q \in \mathcal{H}_p} \underline{\omega}(\|\boldsymbol{\xi}_{pq}\|) \, \xi_i \xi_j \sum_{r \in \mathcal{H}_p} \underline{\lambda}\langle \boldsymbol{\xi}_{pq}, \boldsymbol{\zeta}_{pr} \rangle \, \underline{\omega}(\|\boldsymbol{\zeta}_{pr}\|) \, \zeta_k \zeta_\ell \, \beta_{pr} \, \beta_{pq} \, \Delta V^2 \,, \tag{42}$$

where ξ_i, ξ_j, ξ_k, ξ_ℓ, ζ_k, and ζ_ℓ are the components of the bonds $\boldsymbol{\xi}_{pq} = \mathbf{x}_q - \mathbf{x}_p$ and $\boldsymbol{\zeta}_{pr} = \mathbf{x}_r - \mathbf{x}_p$.

6. Numerical examples

In this section, we verify the proposed peridynamic model for anisotropic materials by means of several numerical examples. The first two examples show that the components of the 2D and 3D elasticity tensor, computed numerically with the proposed PD formulation, are very close to the corresponding components obtained with CCM. The last three numerical examples simulate realistic applications with anisotropic materials. In these last three cases PD solutions are compared to FEM solutions. Differences are unavoidable between the two due to three main reasons:

1. The PD surface effect (see, for example, [72–74]);
2. The way boundary conditions are imposed (see, for example, [88,89]);
3. The fact that PD and CCM in general provide different solutions to the same problem (see, for example, [69,91]).

However, a good agreement between PD and FEM solutions is usually expected.

6.1. Verification of 2D elastic coefficients

Table 1 reports the mechanical properties of an orthotropic material and an isotropic one taken from [5]. The mechanical properties of an orthotropic material are often given in the *material coordinate system*, which is here denoted by 1- and 2-axes. This is, for instance, the case of the components of the elasticity tensor for the composite material in Table 1. However, stresses and strains are evaluated in the *problem coordinate system*, denoted by x- and y-axes, which may be different from the material coordinate system. Therefore, the components of the elasticity tensor in the problem coordinate system vary depending on its orientation with respect to the material coordinate system.

The 2D elasticity tensor for an orthotropic material expressed in the material coordinate system is given as

$$\begin{bmatrix} \sigma_{11} \\ \sigma_{22} \\ \sigma_{12} \end{bmatrix} = \begin{bmatrix} C_{1111} & C_{1122} & 0 \\ \cdot & C_{2222} & 0 \\ \cdot & \cdot & C_{1212} \end{bmatrix} \begin{bmatrix} \varepsilon_{11} \\ \varepsilon_{22} \\ 2\varepsilon_{12} \end{bmatrix}, \tag{43}$$

where, in plane stress conditions,

$$C_{1111} = \frac{E_1}{1 + \nu_{12}\nu_{21}} \,, \tag{44a}$$

$$C_{2222} = \frac{E_2}{1 + \nu_{12}\nu_{21}} \,, \tag{44b}$$

$$C_{1122} = \frac{\nu_{12}\, E_2}{1 + \nu_{12}\nu_{21}} \,, \tag{44c}$$

$$C_{1212} = G_{12} \,, \tag{44d}$$

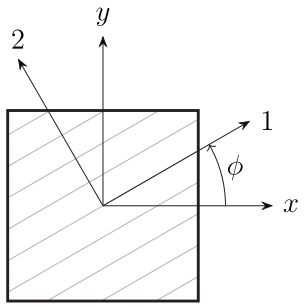

Fig. 6. Rotation by an angle ϕ of the material coordinate system with respect to the problem reference system.

with $\nu_{21} = \nu_{12}E_2/E_1$. By rotating the material coordinate system by an angle ϕ, as shown in Fig. 6, the elasticity tensor in the problem coordinate system [5, ch. 2.3] is expressed as

$$\begin{bmatrix}\sigma_{xx}\\ \sigma_{yy}\\ \sigma_{xy}\end{bmatrix} = \begin{bmatrix}C_{xxxx} & C_{xxyy} & C_{xxxy}\\ \cdot & C_{yyyy} & C_{yyxy}\\ \cdot & \cdot & C_{xyxy}\end{bmatrix}\begin{bmatrix}\epsilon_{xx}\\ \epsilon_{yy}\\ 2\epsilon_{xy}\end{bmatrix}, \tag{45}$$

with

$$C_{xxxx} = c^4C_{1111} + 2c^2s^2(C_{1122} + 2C_{1212}) + s^4C_{2222}\,, \tag{46a}$$
$$C_{yyyy} = c^4C_{2222} + 2c^2s^2(C_{1122} + 2C_{1212}) + s^4C_{1111}\,, \tag{46b}$$
$$C_{xxyy} = (c^4 + s^4)C_{1122} + c^2s^2(C_{1111} + C_{2222} - 4C_{1212})\,, \tag{46c}$$
$$C_{xyxy} = (c^4 + s^4)C_{1212} + c^2s^2(C_{1111} + C_{2222} - 2C_{1122} - 2C_{1212})\,, \tag{46d}$$
$$C_{xxxy} = c^3s(C_{1111} - C_{1122} - 2C_{1212}) - cs^3(C_{2222} - C_{1122} - 2C_{1212})\,, \tag{46e}$$
$$C_{yyxy} = cs^3(C_{1111} - C_{1122} - 2C_{1212}) - c^3s(C_{2222} - C_{1122} - 2C_{1212})\,, \tag{46f}$$

where $c = \cos(\phi)$ and $s = \sin(\phi)$. It is worth noting that the material in the problem coordinate system (for $\phi \neq n\pi/2$ with $n = 0, 1, 2, \dots$) appears to be fully anisotropic.

To obtain the mechanical properties in Eq. (46), we used multiple values for the angle ϕ, one at each interval of $\Delta\phi = 1.8°$. The $\overline{m}$-ratio, defined as the ratio between the horizon size δ and the grid spacing Δx, is equal to 10, which is a relatively high value for this parameter. This choice is driven by the need of reducing the numerical errors due to the numerical integration [86], in order to highlight the possible errors due to the constitutive model of the material. For simplicity, the grid spacing is unitary. Therefore, we compute numerically the peridynamic components of the elasticity tensor for nodes with a complete neighborhood thanks to Eq. (42), and compare the numerical results with the corresponding CCM value given in Eq. (46).

Fig. 7 shows the polar plots of the components of the elasticity tensor, in plane stress conditions, for the different values of the angle ϕ for the composite (orthotropic) material, whose properties are reported in Table 1. Note that the components C_{yyyy} and C_{yyxy} are not shown in Fig. 7 since their polar plots are the same as those of C_{xxxx} and C_{xxxy}, respectively, rotated by 90°. The PD components of the elasticity tensor coincide with the CCM ones, which means that the proposed model is able to capture all the 2D elastic properties of a fully anisotropic material. Furthermore, Fig. 8 shows the polar plots of the components of the elasticity tensor, in plane stress conditions, for an isotropic material (steel), whose mechanical properties are reported in Table 1. Also in this case, the PD stiffness properties coincide with those obtained with CCM.

6.2. Verification of 3D elastic coefficients

Similarly to Section 6.1, we verify the correctness of the PD components of the 3D elasticity tensor for an orthotropic material when the material reference system, denoted by 1-, 2-, and 3-axes, is rotated by an angle ϕ around the 3-axis with respect to the problem reference system, denoted by x-, y-, and z-axes (see Fig. 6). The 3D elasticity tensor for an orthotropic material expressed in the material coordinate system [5] is given as

$$\begin{bmatrix}\sigma_{11}\\ \sigma_{22}\\ \sigma_{33}\\ \sigma_{23}\\ \sigma_{13}\\ \sigma_{12}\end{bmatrix} = \begin{bmatrix}C_{1111} & C_{1122} & C_{1133} & 0 & 0 & 0\\ \cdot & C_{2222} & C_{2233} & 0 & 0 & 0\\ \cdot & \cdot & C_{3333} & 0 & 0 & 0\\ \cdot & \cdot & \cdot & C_{2323} & 0 & 0\\ \cdot & \cdot & \cdot & \cdot & C_{1313} & 0\\ \cdot & \cdot & \cdot & \cdot & \cdot & C_{1212}\end{bmatrix}\begin{bmatrix}\epsilon_{11}\\ \epsilon_{22}\\ \epsilon_{33}\\ 2\epsilon_{23}\\ 2\epsilon_{13}\\ 2\epsilon_{12}\end{bmatrix}, \tag{47}$$

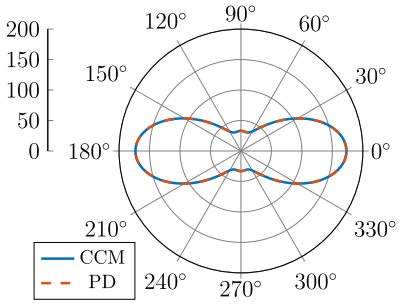

(a) C_{xxxx} [GPa].

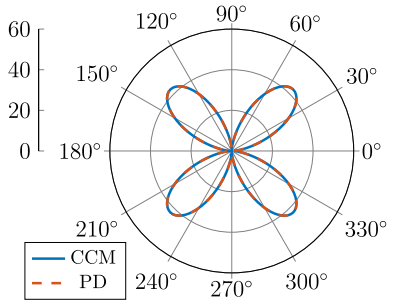

(b) C_{xxyy} [GPa].

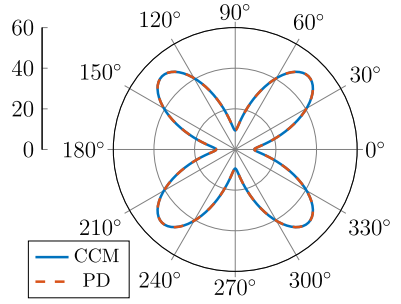

(c) C_{xyxy} [GPa].

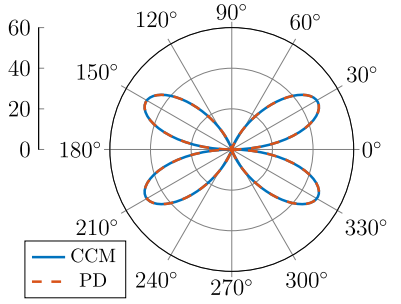

(d) C_{xxxy} [GPa].

Fig. 7. Components of the 2D elasticity tensor for an orthotropic material depending on the angle ϕ between the material and problem reference systems.

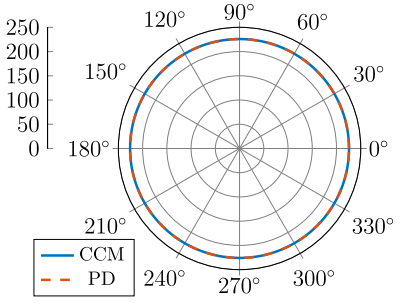

(a) C_{xxxx} [GPa].

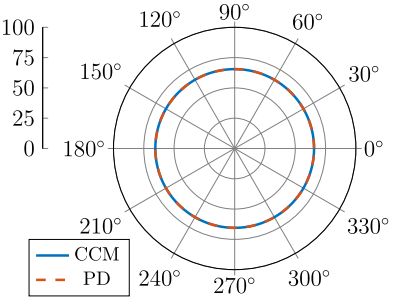

(b) C_{xxyy} [GPa].

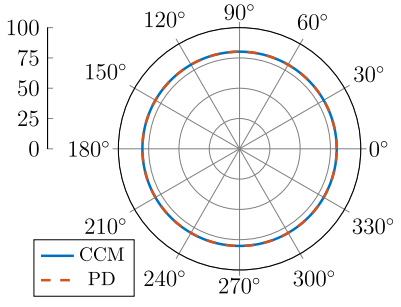

(c) C_{xyxy} [GPa].

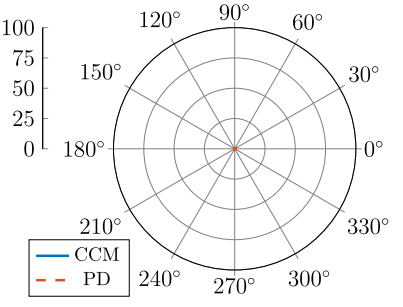

(d) C_{xxxy} [GPa].

Fig. 8. Components of the 2D elasticity tensor for an isotropic material depending on the angle ϕ between the material and problem reference systems.

where

$$C_{1111} = \frac{E_1(1-\nu_{23}\nu_{32})}{1+\nu_{12}\nu_{21}+\nu_{13}\nu_{31}+\nu_{23}\nu_{32}+2\nu_{21}\nu_{31}\nu_{23}}, \tag{48a}$$

$$C_{2222} = \frac{E_2(1-\nu_{13}\nu_{31})}{1+\nu_{12}\nu_{21}+\nu_{13}\nu_{31}+\nu_{23}\nu_{32}+2\nu_{21}\nu_{31}\nu_{23}}, \tag{48b}$$

$$C_{3333} = \frac{E_3(1-\nu_{12}\nu_{21})}{1+\nu_{12}\nu_{21}+\nu_{13}\nu_{31}+\nu_{23}\nu_{32}+2\nu_{21}\nu_{31}\nu_{23}}, \tag{48c}$$

$$C_{1122} = \frac{E_2(\nu_{12}+\nu_{13}\nu_{32})}{1+\nu_{12}\nu_{21}+\nu_{13}\nu_{31}+\nu_{23}\nu_{32}+2\nu_{21}\nu_{31}\nu_{23}}, \tag{48d}$$

$$C_{1133} = \frac{E_3(\nu_{13}+\nu_{12}\nu_{23})}{1+\nu_{12}\nu_{21}+\nu_{13}\nu_{31}+\nu_{23}\nu_{32}+2\nu_{21}\nu_{31}\nu_{23}}, \tag{48e}$$

$$C_{2233} = \frac{E_3(\nu_{23}+\nu_{21}\nu_{13})}{1+\nu_{12}\nu_{21}+\nu_{13}\nu_{31}+\nu_{23}\nu_{32}+2\nu_{21}\nu_{31}\nu_{23}}, \tag{48f}$$

$$C_{1212} = G_{12}, \tag{48g}$$

$$C_{1313} = G_{13}, \tag{48h}$$

$$C_{2323} = G_{23}, \tag{48i}$$

with $\nu_{21} = \nu_{12}E_2/E_1$, $\nu_{31} = \nu_{13}E_3/E_1$, and $\nu_{32} = \nu_{23}E_3/E_2$. The mechanical properties of the composite material in Table 1 are used. For a rotation of an angle ϕ of the material reference system, the elasticity tensor in the problem coordinate system [5, ch. 2.3] is expressed as

$$\begin{bmatrix}\sigma_{xx}\\ \sigma_{yy}\\ \sigma_{zz}\\ \sigma_{yz}\\ \sigma_{xz}\\ \sigma_{xy}\end{bmatrix} = \begin{bmatrix} C_{xxxx} & C_{xxyy} & C_{xxzz} & 0 & 0 & C_{xxxy}\\ \cdot & C_{yyyy} & C_{yyzz} & 0 & 0 & C_{yyxy}\\ \cdot & \cdot & C_{zzzz} & 0 & 0 & C_{zzxy}\\ \cdot & \cdot & \cdot & C_{yzyz} & C_{yzxz} & 0\\ \cdot & \cdot & \cdot & \cdot & C_{xzxz} & 0\\ \cdot & \cdot & \cdot & \cdot & \cdot & C_{xyxy}\end{bmatrix}\begin{bmatrix}\varepsilon_{xx}\\ \varepsilon_{yy}\\ \varepsilon_{zz}\\ 2\varepsilon_{yz}\\ 2\varepsilon_{xz}\\ 2\varepsilon_{xy}\end{bmatrix}, \tag{49}$$

where some components are the same as those obtained in Eq. (46) for the 2D case and the others are given as

$$C_{zzzz} = C_{3333}, \tag{50a}$$

$$C_{xxzz} = c^2C_{1133} + s^2C_{2233}, \tag{50b}$$

$$C_{yyzz} = c^2C_{2233} + s^2C_{1133}, \tag{50c}$$

$$C_{zzxy} = cs(C_{1133} + C_{2233}), \tag{50d}$$

$$C_{xzxz} = c^2C_{1313} + s^2C_{2323}, \tag{50e}$$

$$C_{yzyz} = c^2C_{2323} + s^2C_{1313}, \tag{50f}$$

$$C_{xzyz} = cs(C_{1313} - C_{2323}), \tag{50g}$$

where $c = \cos(\phi)$ and $s = \sin(\phi)$. Note that the material in the problem coordinate system (for $\phi \neq n\pi/2$ with $n = 0, 1, 2, \dots$) behaves as a monoclinic material.

In the numerical model, to reduce the numerical errors due to the numerical integration, we used $\overline{m} = \delta/\Delta x = 10$, with a unitary grid spacing for simplicity. The PD components of the elasticity tensor, obtained with Eq. (42), are compared with the corresponding CCM value given in Eq. (50). Each elastic coefficient is computed for the following values of the angle between the material and problem reference system: $\phi = n\Delta\phi$ with $n = 0, 1, 2, \dots$ and $\Delta\phi = 1.8°$.

Fig. 9 shows the polar plots of the components of the elasticity tensor for the composite (orthotropic) material, whose properties are reported in Table 1. It is worth noting that the components C_{xxxx}, C_{xxyy}, C_{xyxy}, and C_{xxxy} are not shown here since their plots are almost identical to those of the 2D case in Fig. 7 (the shape is exactly the same, only the values of the components of the elasticity tensor in the material reference system are slightly different). The plots of the components C_{yyzz} and C_{yzyz} can be obtained by rotating the plots of C_{xxzz} and C_{xzxz} by 90°. Furthermore, the component C_{zzzz} is not plotted since it has a constant value when varying ϕ (see Eq. (50a)).

As evident in Fig. 9, the components of the 3D elasticity tensor computed by means of the PD numerical model coincide with those obtained with CCM. The components of the elasticity tensor that were not considered in this analysis, i.e., the components that are equal to 0 in Eq. (49), can be verified by rotating the material reference system about the x-axis and y-axis. By doing so, plots similar to those shown in Fig. 9 can be obtained. Therefore, all 21 elastic coefficients can be modeled by the proposed formulation for anisotropic materials. Clearly, since monoclinic, orthotropic, transversely isotropic, and isotropic materials are special cases of fully anisotropic materials, they can be modeled with the proposed method as well.

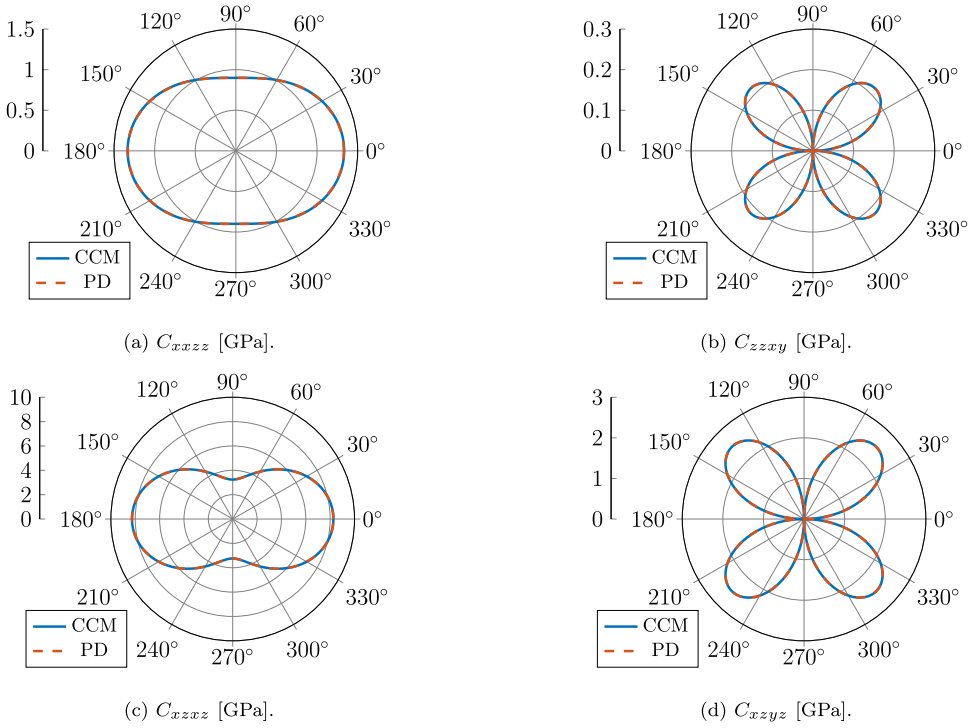

(a) C_{xxzz} [GPa]. (b) C_{zzxy} [GPa].

(c) C_{xzxz} [GPa]. (d) C_{xzyz} [GPa].

Fig. 9. Components of the 3D elasticity tensor for an orthotropic material depending on the angle ϕ between the material and problem reference systems.

Table 2
Properties of an orthotropic material (glass fiber-epoxy matrix composite material) [92].

Elastic moduli	Shear modulus	Poisson's ratio
$E_1 = 44\,\text{GPa}$ $E_2 = 10.5\,\text{GPa}$	$G_{12} = 3.74\,\text{GPa}$	$\nu_{12} = 0.36$

6.3. Plate under traction on half edge

In this section, we numerically solve a 2D problem of a plate made of a single ply of glass fiber-epoxy matrix composite material under plane stress conditions. The mechanical properties of this orthotropic material are reported in Table 2. The elasticity tensor is obtained by substituting the material properties into Eqs. (43) and (44). The material reference system is rotated by an angle $\phi = 40°$ with respect to the problem reference system. Therefore, since Eqs. (45) and (46) are used to compute the elasticity tensor in the problem reference system, the material appears to be fully anisotropic.

The geometry and the boundary conditions of the plate are shown in Fig. 10. The plate has the dimensions $\ell_x = 0.3\,\text{m}$ and $\ell_y = 0.2\,\text{m}$, and its thickness is $t = 0.001\,\text{m}$. The plate is clamped on the left edge and a traction load in x direction $\overline{p}_x = 10\,\text{MPa}$ is applied on the upper half of the right edge. The constraints on the left edge of the plate are imposed over a fictitious layer outside the body (the blue region in Fig. 10), whereas the applied load is equally distributed over the nodes within a region of the body close to the boundary (the red region in Fig. 10).

The plate is discretized with a uniform grid of nodes with an equal spacing $\Delta x = 0.001\,\text{m}$ in both directions. Therefore, the total number of nodes of the 2D peridynamic model is $300 \times 200 = 60\,000$. The $\overline{m}$-ratio is chosen as $\overline{m} = \delta/\Delta x = 5$. To obtain a reference solution, the same problem is solved by means of the finite element method (FEM). For the FEM analysis, quadrilateral (square) elements with sides of $\Delta x/2 = 0.0005\,\text{m}$ are used. Therefore, the magnitude of the relative difference between PD and FEM is evaluated at each peridynamic node as

$$\epsilon = \frac{\sqrt{\left(u_x^{PD} - u_x^{FEM}\right)^2 + \left(u_y^{PD} - u_y^{FEM}\right)^2}}{\max\left(\sqrt{\left(u_x^{FEM}\right)^2 + \left(u_y^{FEM}\right)^2}\right)}, \tag{51}$$

where $\mathbf{u}^{PD}$ and $\mathbf{u}^{FEM}$ are the displacement fields computed with PD and FEM, respectively.

Fig. 11 shows the deformed shapes obtained with the FEM and PD solutions. It is evident that the two solutions are similar. The magnitude of the relative difference, computed with Eq. (51) and shown in Fig. 12, is indeed smaller than 1% in the whole body.

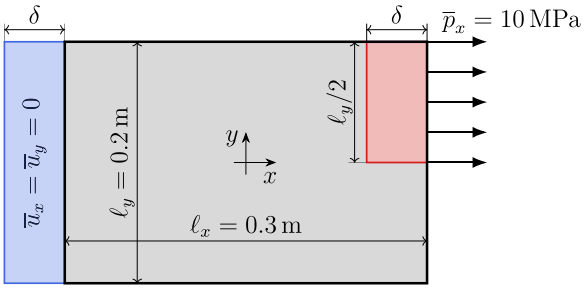

Fig. 10. Geometry and boundary conditions for the problem of a plate under traction on half edge. (For interpretation of the references to color in this figure legend, the reader is referred to the web version of this article.)

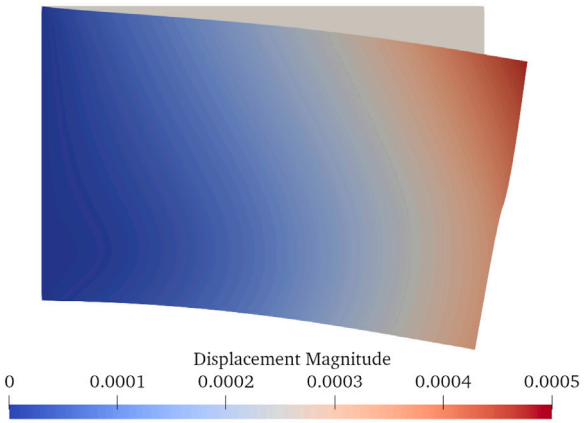

(a) FEM solution of the displacement field in meters.

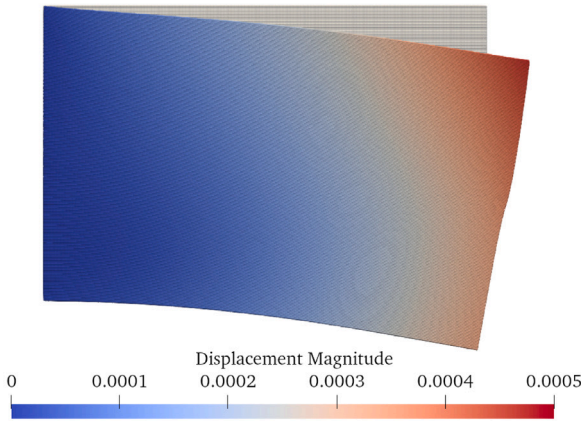

(b) PD solution of the displacement field in meters.

Fig. 11. Deformed shape of a plate under traction on half edge magnified by a scale factor of 50 for the FEM and PD solution.

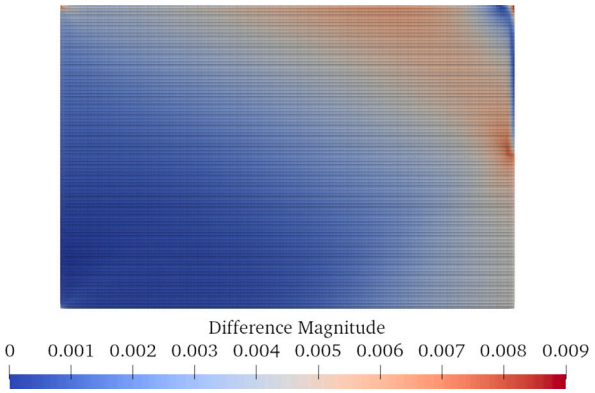

Fig. 12. Magnitude of the relative differences between PD and FEM solutions for a plate under traction on half edge.

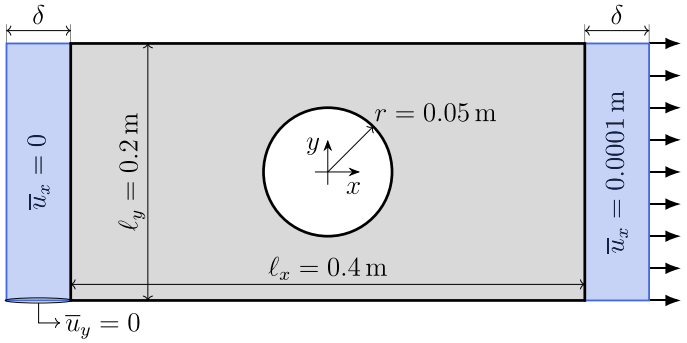

Fig. 13. Geometry and boundary conditions for the problem of a plate with hole under traction.

Note that the highest differences are located at nodes close to the boundary where the PD solution is affected by the surface effect (see Remark 4) and the simplified way of imposing nonlocal boundary conditions.

6.4. Plate with hole under traction

Similarly to the previous section, we address a 2D problem of a plate with a central hole under plane stress conditions. The material properties are the same as those in the previous example (see Table 2), but the rotation of the material reference system is $\phi = -25°$ with respect to the problem reference system. Fig. 13 shows the geometry of the plate with dimensions $\ell_x = 0.4\,\mathrm{m}$ and $\ell_y = 0.2\,\mathrm{m}$, and thickness $t = 0.001\,\mathrm{m}$. The central hole is a circle of radius $r = 0.05\,\mathrm{m}$. The plate is subjected to traction by constraining the displacements $\overline{u}_x = 0$ in x direction of a fictitious layer close to the left edge and by moving of $\overline{u}_x = 0.0001\,\mathrm{m}$ a fictitious layer close to the right edge, as shown in Fig. 13. Furthermore, the lower side of the fictitious layer close to the left edge is constrained in y direction.

The uniform grid spacing is $\Delta x = 0.001\,\mathrm{m}$ and the total number of nodes is 72 140. The $\overline{m}$-ratio is chosen as $\overline{m} = \delta/\Delta x = 5$. The magnitude of the relative difference is evaluated with Eq. (51) by comparing the PD solution with the FEM one, obtained with quadrilateral (square) elements with sides of $\Delta x/2 = 0.0005\,\mathrm{m}$.

The deformed shapes for the FEM and PD solutions, shown in Fig. 14, are similar. In particular, the influence of the component C_{xxxy} of the elasticity tensor can be seen in Fig. 14 since the shear deformation is triggered by a traction in x direction. Fig. 15 shows the magnitude of the relative difference at each peridynamic node, which is smaller than 3% in the whole body.

6.5. 3D bar under traction

In this section, we deal with the problem of a 3D bar under traction made of polyphenylene sulfide (PPS) reinforced with 40% weight of carbon fibers. The components of the elasticity tensor in the material reference system are reported in Table 3. The material is rotated by an angle $\phi = 30°$ in the xy plane, and the components of the elasticity tensor used to solve the problem are computed with Eqs. (46) and (50). Therefore, the material appears to be monoclinic in the problem reference system (see Eq. (49)).

The dimensions of the 3D bar are $\ell_x = 0.6\,\mathrm{m}$, $\ell_y = 0.15\,\mathrm{m}$, and $\ell_z = 0.12\,\mathrm{m}$. As shown in Fig. 16, one end of the bar is clamped and the other one is displaced in x direction by $\overline{u}_x = 0.001\,\mathrm{m}$. In the peridynamic model, these constraints are imposed over two fictitious layers close to the ends of the bar. The body is discretized with a uniform grid of nodes with a constant spacing $\Delta x = 0.01\,\mathrm{m}$ in all

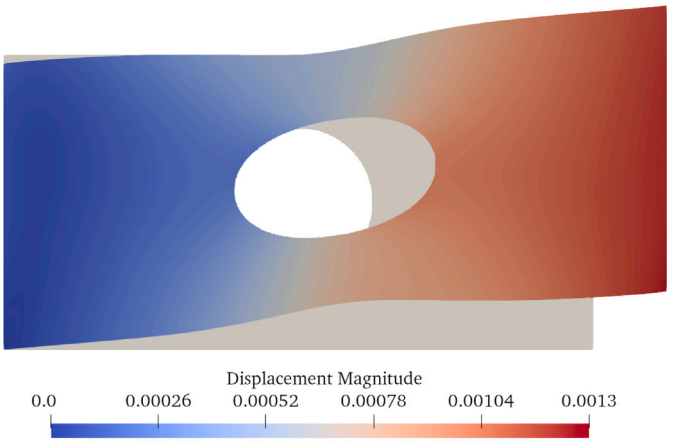

(a) FEM solution of the displacement field in meters.

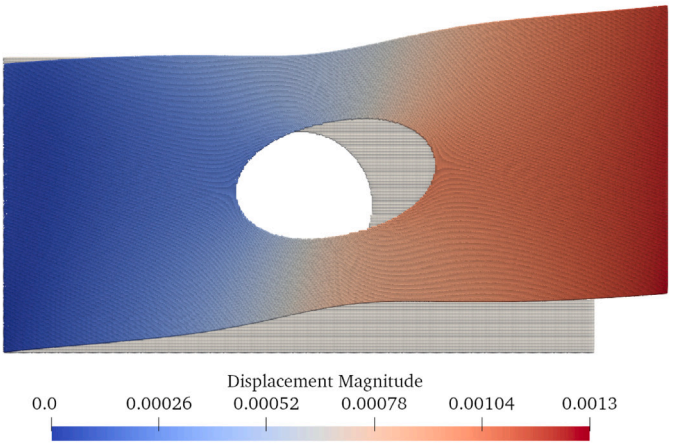

(b) PD solution of the displacement field in meters.

Fig. 14. Deformed shape of a plate with a hole under traction magnified by a scale factor of 50 for the FEM and PD solution.

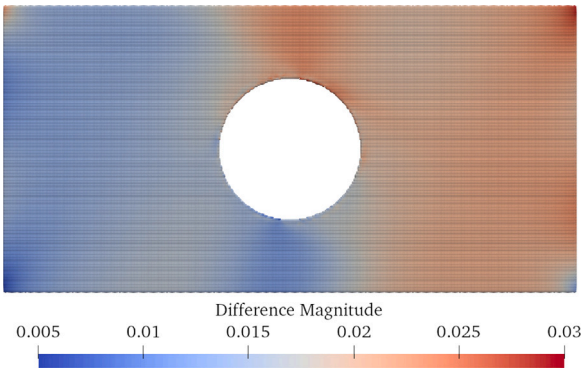

Fig. 15. Magnitude of the relative difference between PD and FEM solutions for a plate with a hole under traction.

Table 3
Properties of an orthotropic material (PPS reinforced with 40% weight of carbon fibers) [93].

Components of elasticity tensor		
$C_{1111} = 36\,\text{GPa}$	$C_{2222} = 15.1\,\text{GPa}$	$C_{3333} = 10.9\,\text{GPa}$
$C_{2233} = 6.3\,\text{GPa}$	$C_{1133} = 6.4\,\text{GPa}$	$C_{1122} = 6.7\,\text{GPa}$
$C_{2323} = 2.78\,\text{GPa}$	$C_{1313} = 3.28\,\text{GPa}$	$C_{1212} = 5.8\,\text{GPa}$

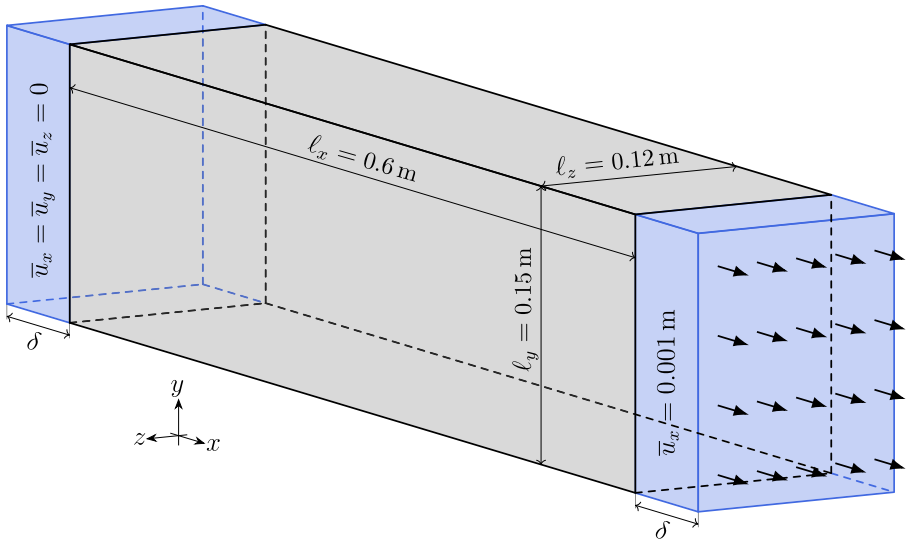

Fig. 16. Geometry and boundary conditions for the problem of a 3D bar under traction.

directions, for a total number of nodes equal to 10 800. The $\overline{m}$-ratio is chosen as $\overline{m} = \delta/\Delta x = 3$. A reference solution is obtained by solving the same problem by means of FEM with hexahedral (cubic) elements with edges of $\Delta x/2 = 0.005\,\text{m}$, so that the magnitude of the relative difference can be evaluated at each peridynamic node as

$$\epsilon = \frac{\sqrt{\left(u_x^{PD} - u_x^{FEM}\right)^2 + \left(u_y^{PD} - u_y^{FEM}\right)^2 + \left(u_z^{PD} - u_z^{FEM}\right)^2}}{\max\left(\sqrt{\left(u_x^{FEM}\right)^2 + \left(u_y^{FEM}\right)^2 + \left(u_z^{FEM}\right)^2}\right)}, \tag{52}$$

where $\mathbf{u}^{PD}$ and $\mathbf{u}^{FEM}$ are the displacement fields computed with PD and FEM, respectively.

The FEM and PD solutions are shown Fig. 17. It is clear that the PD model is able to reproduce the components of the elasticity tensor in excellent agreement with a model based on FEM. For instance, it is worth noting that, in both models, there is a deformation in y direction due to shear strain in xy plane, which is triggered by the non-zero component C_{xxxy} of the elasticity tensor and the traction in x direction. The magnitude of the relative differences, evaluated with Eq. (52), is shown in Fig. 18. The maximum magnitude of the relative differences remains below 3% in all peridynamic nodes.

7. Conclusions

For the first time, a general ordinary state-based peridynamic formulation to model anisotropic materials in 2D and 3D was proposed in this work. The novelty of this formulation is the introduction of two distinct bond stiffness functions, i.e., the *single-bond micromodulus* and the *double-bond micromodulus*. The former depends on the orientation of a single bond, whereas the latter depends on the orientations of a pair of bonds. These micromoduli were calibrated such that the components of the elasticity tensor evaluated with the proposed formulation exactly match those of classical continuum mechanics in the case of homogeneous deformation. The new formulation is validated by several numerical examples in 2D and 3D, highlighting the excellent agreement of the PD results with FEM solutions.

The proposed formulation is suitable to model fully anisotropic materials, which is the most general type of material in nature. Since monoclinic, orthotropic, transversely isotropic, and isotropic materials are special cases of fully anisotropic ones, they can be modeled with the proposed constitutive model as well.

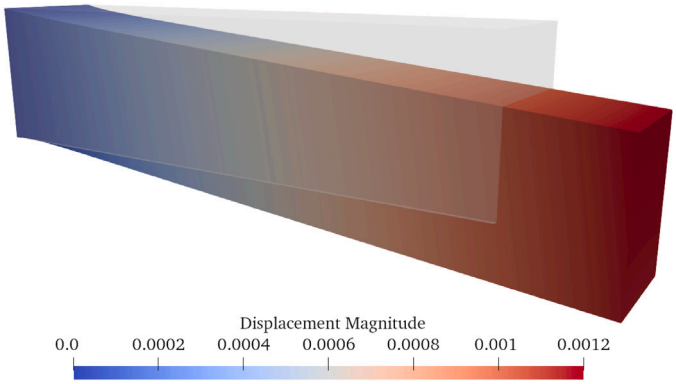

(a) FEM solution of the displacement field in meters.

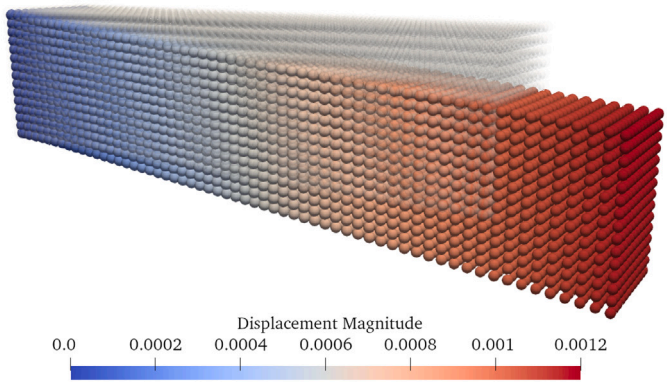

(b) PD solution of the displacement field in meters.

Fig. 17. Deformed shape of a 3D bar under traction magnified by a scale factor of 100 for the FEM and PD solution.

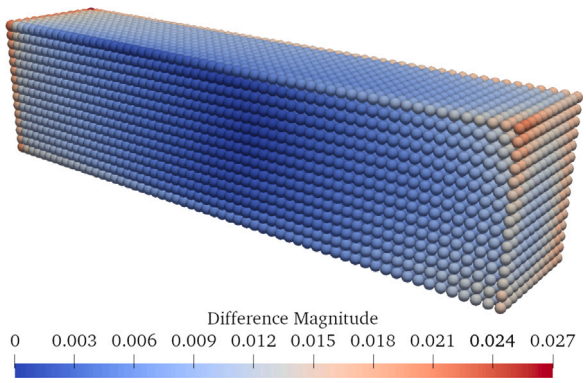

Fig. 18. Magnitude of the relative difference between PD and FEM solutions for a 3D bar under traction.

CRediT authorship contribution statement

Francesco Scabbia: Writing – original draft, Visualization, Validation, Software, Methodology, Investigation, Formal analysis, Data curation, Conceptualization. **Mirco Zaccariotto:** Writing – review & editing, Supervision, Resources, Project administration, Funding acquisition. **Ugo Galvanetto:** Writing – review & editing, Supervision, Resources, Project administration, Funding acquisition.

Declaration of competing interest

The authors declare that they have no known competing financial interests or personal relationships that could have appeared to influence the work reported in this paper.

Data availability

Data will be made available on request.

Acknowledgments

The authors acknowledge support from the European Union - Next GenerationEU under the call PRIN 2022 PNRR of the Italian Minister of University and Research (MUR); Project P2022HLHHB (PE - Physical Sciences and Engineering) A digital framework for the cutting of soft tissues: A first step towards virtual surgery (National coordinator V.D.), and from University of Padova, Italy under the research projects BIRD2023 NR.237212/23 and NR.232492/23.

Declaration of competing interest

The authors declare that they have no known competing financial interests or personal relationships that could have appeared to influence the work reported in this paper.

Appendix A. Derivation of the force density vector state and elasticity tensor in the new formulation

In ordinary state-based peridynamics [12], the magnitude of the force density vector state is defined as the Fréchet derivative of the peridynamic strain energy density with respect to the extension scalar state:

$$\|\underline{\mathbf{T}}\langle\boldsymbol{\xi}\rangle\| = \nabla W(\underline{e})\,. \tag{A.1}$$

The definition of Fréchet derivative [12] applied to W as a function of the extension scalar state $\underline{e}$ is given as

$$W(\underline{e}+d\underline{e}) = W(\underline{e}) + \int_{\mathcal{H}_{\mathbf{x}}} \nabla W(\underline{e}\langle\boldsymbol{\xi}\rangle)\, d\underline{e}\langle\boldsymbol{\xi}\rangle \mathrm{d}V_{\mathbf{x}'} + o(\|d\underline{e}\|)\,, \tag{A.2}$$

where $d\underline{e}$ is an increment of the extension scalar state and $\boldsymbol{\xi} = \mathbf{x}' - \mathbf{x}$. The definition of strain energy density (Eq. (22)) in the new formulation of ordinary state-based peridynamics for anisotropic materials yields

$$\begin{aligned}
W(\underline{e}+d\underline{e}) &= \frac{1}{2m}\int_{\mathcal{H}_{\mathbf{x}}} \underline{k}\langle\boldsymbol{\xi}\rangle\, \underline{\omega}(\|\boldsymbol{\xi}\|)\left(\underline{e}\langle\boldsymbol{\xi}\rangle + d\underline{e}\langle\boldsymbol{\xi}\rangle\right)^2 \mathrm{d}V_{\mathbf{x}'} \\
&\quad + \frac{1}{2m^2}\int_{\mathcal{H}_{\mathbf{x}}}\int_{\mathcal{H}_{\mathbf{x}}} \underline{\lambda}\langle\boldsymbol{\xi},\boldsymbol{\zeta}\rangle\, \underline{\omega}(\|\boldsymbol{\xi}\|)\,\underline{\omega}(\|\boldsymbol{\zeta}\|)\,\|\boldsymbol{\xi}\|\,\|\boldsymbol{\zeta}\| \left(\underline{e}\langle\boldsymbol{\xi}\rangle + d\underline{e}\langle\boldsymbol{\xi}\rangle\right)\left(\underline{e}\langle\boldsymbol{\zeta}\rangle + d\underline{e}\langle\boldsymbol{\zeta}\rangle\right) \mathrm{d}V_{\mathbf{x}''}\mathrm{d}V_{\mathbf{x}'} \\
&= W(\underline{e}) + \frac{1}{m}\int_{\mathcal{H}_{\mathbf{x}}} \underline{k}\langle\boldsymbol{\xi}\rangle\, \underline{\omega}(\|\boldsymbol{\xi}\|)\, \underline{e}\langle\boldsymbol{\xi}\rangle\, d\underline{e}\langle\boldsymbol{\xi}\rangle \mathrm{d}V_{\mathbf{x}'} \\
&\quad + \frac{1}{2m^2}\int_{\mathcal{H}_{\mathbf{x}}}\int_{\mathcal{H}_{\mathbf{x}}} \underline{\lambda}\langle\boldsymbol{\xi},\boldsymbol{\zeta}\rangle\, \underline{\omega}(\|\boldsymbol{\xi}\|)\,\underline{\omega}(\|\boldsymbol{\zeta}\|)\,\|\boldsymbol{\xi}\|\,\|\boldsymbol{\zeta}\|\, \underline{e}\langle\boldsymbol{\zeta}\rangle\, d\underline{e}\langle\boldsymbol{\xi}\rangle \mathrm{d}V_{\mathbf{x}''}\mathrm{d}V_{\mathbf{x}'} \\
&\quad + \frac{1}{2m^2}\int_{\mathcal{H}_{\mathbf{x}}}\int_{\mathcal{H}_{\mathbf{x}}} \underline{\lambda}\langle\boldsymbol{\xi},\boldsymbol{\zeta}\rangle\, \underline{\omega}(\|\boldsymbol{\zeta}\|)\,\underline{\omega}(\|\boldsymbol{\xi}\|)\,\|\boldsymbol{\zeta}\|\,\|\boldsymbol{\xi}\|\, \underline{e}\langle\boldsymbol{\zeta}\rangle\, d\underline{e}\langle\boldsymbol{\xi}\rangle \mathrm{d}V_{\mathbf{x}''}\mathrm{d}V_{\mathbf{x}'} + o(\|d\underline{e}\|)\,,
\end{aligned} \tag{A.3}$$

where in the last double integral the integration variables are interchanged ($\boldsymbol{\xi} \leftrightarrow \boldsymbol{\zeta}$). As we shall see later, the stiffness coefficient $\underline{\lambda}\langle\boldsymbol{\xi},\boldsymbol{\zeta}\rangle$ must be chosen to satisfy the condition $\underline{\lambda}\langle\boldsymbol{\xi},\boldsymbol{\zeta}\rangle = \underline{\lambda}\langle\boldsymbol{\zeta},\boldsymbol{\xi}\rangle$ in order for the PD elasticity tensor to have the major symmetry. Thanks to this property, the last two double integrals in Eq. (A.3) are equal to each other, and the force density vector state is thus given as

$$\underline{\mathbf{T}}\langle\boldsymbol{\xi}\rangle = \frac{\underline{\omega}(\|\boldsymbol{\xi}\|)}{m}\left[\underline{k}\langle\boldsymbol{\xi}\rangle\, \underline{e}\langle\boldsymbol{\xi}\rangle + \frac{1}{m}\,\|\boldsymbol{\xi}\| \int_{\mathcal{H}_{\mathbf{x}}} \underline{\lambda}\langle\boldsymbol{\xi},\boldsymbol{\zeta}\rangle\, \underline{\omega}(\|\boldsymbol{\zeta}\|)\,\|\boldsymbol{\zeta}\|\, \underline{e}\langle\boldsymbol{\zeta}\rangle \mathrm{d}V_{\mathbf{x}''}\right] \underline{\mathbf{M}}\langle\boldsymbol{\xi}\rangle\,. \tag{A.4}$$

Assuming that the deformation is small, i.e., $\underline{\mathbf{U}}\langle\boldsymbol{\xi}\rangle \ll \delta$, the extension scalar state (Eq. (10)) and the direction vector state (Eq. (11)) are respectively simplified as $\underline{e}\langle\boldsymbol{\xi}\rangle = \underline{\mathbf{U}}\langle\boldsymbol{\xi}\rangle \cdot \underline{\mathbf{M}}\langle\boldsymbol{\xi}\rangle$ and $\underline{\mathbf{M}}\langle\boldsymbol{\xi}\rangle = \boldsymbol{\xi}/\|\boldsymbol{\xi}\|$. Thus, the force density vector state can be linearized as follows [66]:

$$\underline{\mathbf{T}}[\mathbf{x},t]\langle\boldsymbol{\xi}\rangle = \int_{\mathcal{H}_{\mathbf{x}}} \underline{\mathbb{K}}[\mathbf{x}]\langle\boldsymbol{\xi},\boldsymbol{\zeta}\rangle\, \underline{\mathbf{U}}[\mathbf{x},t]\langle\boldsymbol{\zeta}\rangle \mathrm{d}V_{\mathbf{x}''}\,, \tag{A.5}$$

where $\underline{\underline{\mathbb{K}}}$ is the *modulus state*, i.e., a double state (a state applied to a pair of bonds). The modulus state is defined as the Fréchet derivative of the force density vector state with respect to the displacement vector state:

$$\underline{\underline{\mathbb{K}}} = \nabla \underline{\mathbf{T}}(\underline{\mathbf{U}}) \,, \tag{A.6}$$

where $\underline{\mathbf{T}}(\underline{\mathbf{U}})$ is derived from Eq. (A.4) as

$$\underline{\mathbf{T}}(\underline{\mathbf{U}}) = \left[\frac{1}{m} \underline{k}\langle\xi\rangle \, \underline{\omega}(\|\xi\|) \, \underline{\mathbf{U}}\langle\xi\rangle \cdot \underline{\mathbf{M}}\langle\xi\rangle + \frac{1}{m^2} \underline{\omega}(\|\xi\|) \, \|\xi\| \int_{\mathcal{H}_\mathbf{x}} \underline{\lambda}\langle\xi,\zeta\rangle \, \underline{\omega}(\|\zeta\|) \, \|\zeta\| \, \underline{\mathbf{U}}\langle\zeta\rangle \cdot \underline{\mathbf{M}}\langle\zeta\rangle \mathrm{d}V_{\mathbf{x}''} \right] \underline{\mathbf{M}}\langle\xi\rangle \,. \tag{A.7}$$

The definition of Fréchet derivative [12] applied to $\underline{\mathbf{T}}$ as a function of the displacement vector state $\underline{\mathbf{U}}$ is given as

$$\underline{\mathbf{T}}(\underline{\mathbf{U}} + d\underline{\mathbf{U}}) = \underline{\mathbf{T}}(\underline{\mathbf{U}}) + \int_{\mathcal{H}_\mathbf{x}} \nabla \underline{\mathbf{T}}(\underline{\mathbf{U}}\langle\zeta\rangle) \, d\underline{\mathbf{U}}\langle\zeta\rangle \mathrm{d}V_{\mathbf{x}''} + o(\|d\underline{\mathbf{U}}\|) \,, \tag{A.8}$$

where $d\underline{\mathbf{U}}$ is an increment of the displacement vector state and $\boldsymbol{\zeta} = \mathbf{x}'' - \mathbf{x}$. To express the first term in the right-hand side of Eq. (A.7) as a function of $\underline{\mathbf{U}}\langle\boldsymbol{\zeta}\rangle$, the Dirac delta function is defined as

$$\Delta(\boldsymbol{\zeta} - \boldsymbol{\xi}) = \begin{cases} 1 & \text{if } \boldsymbol{\zeta} - \boldsymbol{\xi} = \mathbf{0} \,, \\ 0 & \text{otherwise.} \end{cases} \tag{A.9}$$

Therefore, the force density vector state due to the increment $d\underline{\mathbf{U}}\langle\boldsymbol{\zeta}\rangle$ is given as

$$\begin{aligned} \underline{\mathbf{T}}(\underline{\mathbf{U}} + d\underline{\mathbf{U}}) &= \left[\frac{1}{m} \underline{k}\langle\xi\rangle \, \underline{\omega}(\|\xi\|) \int_{\mathcal{H}_\mathbf{x}} \Delta(\boldsymbol{\zeta} - \boldsymbol{\xi}) (\underline{\mathbf{U}}\langle\zeta\rangle + d\underline{\mathbf{U}}\langle\zeta\rangle) \cdot \underline{\mathbf{M}}\langle\zeta\rangle \mathrm{d}V_{\mathbf{x}''} \right. \\ &\quad \left. + \frac{1}{m^2} \underline{\omega}(\|\xi\|) \, \|\xi\| \int_{\mathcal{H}_\mathbf{x}} \underline{\lambda}\langle\xi,\zeta\rangle \, \underline{\omega}(\|\zeta\|) \, \|\zeta\| (\underline{\mathbf{U}}\langle\zeta\rangle + d\underline{\mathbf{U}}\langle\zeta\rangle) \cdot \underline{\mathbf{M}}\langle\zeta\rangle \mathrm{d}V_{\mathbf{x}''} \right] \underline{\mathbf{M}}\langle\xi\rangle \\ &= \underline{\mathbf{T}}(\underline{\mathbf{U}}) + \int_{\mathcal{H}_\mathbf{x}} \left[\frac{1}{m} \underline{k}\langle\xi\rangle \, \underline{\omega}(\|\xi\|) \, \Delta(\boldsymbol{\zeta} - \boldsymbol{\xi}) \, d\underline{\mathbf{U}}\langle\zeta\rangle \cdot \underline{\mathbf{M}}\langle\zeta\rangle \right. \\ &\quad \left. + \frac{1}{m^2} \underline{\lambda}\langle\xi,\zeta\rangle \, \underline{\omega}(\|\xi\|) \, \underline{\omega}(\|\zeta\|) \, \|\xi\| \, \|\zeta\| \, d\underline{\mathbf{U}}\langle\zeta\rangle \cdot \underline{\mathbf{M}}\langle\zeta\rangle \right] \underline{\mathbf{M}}\langle\xi\rangle \mathrm{d}V_{\mathbf{x}''} + o(\|d\underline{\mathbf{U}}\|) \,. \end{aligned} \tag{A.10}$$

The modulus state is then computed as

$$\underline{\underline{\mathbb{K}}}\langle\xi,\zeta\rangle = \frac{\underline{\omega}(\|\xi\|)}{m} \left[\underline{k}\langle\xi\rangle \, \frac{\Delta(\boldsymbol{\zeta} - \boldsymbol{\xi})}{\|\xi\| \, \|\zeta\|} + \frac{1}{m} \underline{\lambda}\langle\xi,\zeta\rangle \, \underline{\omega}(\|\zeta\|) \right] \xi \otimes \zeta \,, \tag{A.11}$$

where $\otimes$ indicates a dyadic product. The coefficients of the PD elasticity tensor are given as [66]

$$\begin{aligned} C_{ijk\ell} &= \int_{\mathcal{H}_\mathbf{x}} \int_{\mathcal{H}_\mathbf{x}} \underline{K}_{ik}\langle\xi,\zeta\rangle \, \xi_j \, \zeta_\ell \mathrm{d}V_{\mathbf{x}''} \mathrm{d}V_{\mathbf{x}'} \\ &= \int_{\mathcal{H}_\mathbf{x}} \int_{\mathcal{H}_\mathbf{x}} \frac{\underline{\omega}(\|\xi\|)}{m} \left[\underline{k}\langle\xi\rangle \, \frac{\Delta(\boldsymbol{\zeta} - \boldsymbol{\xi})}{\|\xi\| \, \|\zeta\|} + \frac{1}{m} \underline{\lambda}\langle\xi,\zeta\rangle \, \underline{\omega}(\|\zeta\|) \right] \xi_i \xi_j \, \zeta_k \zeta_\ell \mathrm{d}V_{\mathbf{x}''} \mathrm{d}V_{\mathbf{x}'} \,, \end{aligned} \tag{A.12}$$

where $\underline{K}_{ik}$ are the components of the modulus state. Eq. (A.12) can be simplified by using the definition in Eq. (A.9) as

$$C_{ijk\ell}(\mathbf{x}) = \frac{1}{m} \int_{\mathcal{H}_\mathbf{x}} \underline{k}\langle\xi\rangle \, \underline{\omega}(\|\xi\|) \frac{\xi_i \xi_j \xi_k \xi_\ell}{\|\xi\|^2} \mathrm{d}V_{\mathbf{x}'} + \frac{1}{m^2} \int_{\mathcal{H}_\mathbf{x}} \int_{\mathcal{H}_\mathbf{x}} \underline{\lambda}\langle\xi,\zeta\rangle \, \underline{\omega}(\|\xi\|) \, \underline{\omega}(\|\zeta\|) \, \xi_i \xi_j \, \zeta_k \zeta_\ell \mathrm{d}V_{\mathbf{x}''} \mathrm{d}V_{\mathbf{x}'} \,. \tag{A.13}$$

The peridynamic elasticity tensor must satisfy the minor and major symmetries as in classical continuum mechanics (see Section 2). The minor symmetries ($C_{ijk\ell} = C_{jik\ell} = C_{ij\ell k}$) are satisfied because switching the order of the indices i and j, or k and ℓ, does not make any difference in the computation of the peridynamic integrals. The major symmetry ($C_{ijk\ell} = C_{k\ell ij}$) is satisfied by the first term on the right-hand side of Eq. (A.13), for which the order of the indices is irrelevant during integration, but it is not necessarily satisfied by the second term. To obtain the condition for the major symmetry of the PD elasticity tensor, we write the latter term for $C_{k\ell ij}$ and interchange the integration variables ($\boldsymbol{\xi} \leftrightarrow \boldsymbol{\zeta}$):

$$\frac{1}{m^2} \int_{\mathcal{H}_\mathbf{x}} \int_{\mathcal{H}_\mathbf{x}} \underline{\lambda}\langle\xi,\zeta\rangle \, \underline{\omega}(\|\xi\|) \, \underline{\omega}(\|\zeta\|) \, \xi_k \xi_\ell \, \zeta_i \zeta_j \mathrm{d}V_{\mathbf{x}''} \mathrm{d}V_{\mathbf{x}'} = \frac{1}{m^2} \int_{\mathcal{H}_\mathbf{x}} \int_{\mathcal{H}_\mathbf{x}} \underline{\lambda}\langle\zeta,\xi\rangle \, \underline{\omega}(\|\zeta\|) \, \underline{\omega}(\|\xi\|) \, \zeta_k \zeta_\ell \, \xi_i \xi_j \mathrm{d}V_{\mathbf{x}''} \mathrm{d}V_{\mathbf{x}'} \,. \tag{A.14}$$

Therefore, by comparing the corresponding terms in Eqs. (A.13) and (A.14) the major symmetry of the PD elasticity tensor is satisfied if $\underline{\lambda}\langle\xi,\zeta\rangle = \underline{\lambda}\langle\zeta,\xi\rangle$.

Appendix B. Computation of the components of the 2D elasticity tensor

Hereinafter, we will compute the PD components of the 2D elasticity tensor with Eq. (26) by considering a complete neighborhood. Thanks to the symmetry of the integration domain, the integral of terms with at least one odd power of any component of the bond is zero. Therefore, the non-null integrals that appear in Eq. (26) for a 2D peridynamic model are the following ones:

$$\int_{\mathcal{H}_\mathbf{x}} \frac{\underline{\omega}(\|\xi\|)}{\|\xi\|^2} \xi_1^2 \xi_2^2 \mathrm{d}V_{\mathbf{x}'} = \frac{m}{8} \,, \tag{B.1a}$$

$$\int_{\mathcal{H}_{\mathbf{x}}} \frac{\omega(\|\boldsymbol{\xi}\|)}{\|\boldsymbol{\xi}\|^6} \xi_p^8 \mathrm{d}V_{\mathbf{x}'} = \frac{35m}{128} \qquad \text{with } p = x, y, \tag{B.1b}$$

$$\int_{\mathcal{H}_{\mathbf{x}}} \frac{\omega(\|\boldsymbol{\xi}\|)}{\|\boldsymbol{\xi}\|^6} \xi_p^6 \xi_q^2 \mathrm{d}V_{\mathbf{x}'} = \frac{5m}{128} \qquad \text{with } p, q = x, y \text{ and } p \neq q, \tag{B.1c}$$

$$\int_{\mathcal{H}_{\mathbf{x}}} \frac{\omega(\|\boldsymbol{\xi}\|)}{\|\boldsymbol{\xi}\|^6} \xi_1^4 \xi_2^4 \mathrm{d}V_{\mathbf{x}'} = \frac{3m}{128}, \tag{B.1d}$$

where the definition of the weighted volume m in Eq. (13) was used. These integrals are solved by employing polar coordinates.

By substituting the bond micromoduli in Eqs. (28) and (29) into the formula for the computation of the components of the PD elasticity tensor in Eq. (26) and using the solutions to the integrals in Eq. (B.1), we obtain the following system of equations:

$$C_{xxxx} = \frac{35}{128} k_{xxxx} + \frac{5}{128} k_{xxyy} + \frac{3}{128} k_{yyyy}, \tag{B.2a}$$

$$C_{xxyy} = \frac{5}{128} k_{xxxx} + \frac{3}{128} k_{xxyy} + \frac{5}{128} k_{yyyy}, \tag{B.2b}$$

$$C_{yyyy} = \frac{3}{128} k_{xxxx} + \frac{5}{128} k_{xxyy} + \frac{35}{128} k_{yyyy}, \tag{B.2c}$$

$$C_{xxxy} = \frac{5}{128} k_{xxxy} + \frac{3}{128} k_{yyxy}, \tag{B.2d}$$

$$C_{yyxy} = \frac{3}{128} k_{xxxy} + \frac{5}{128} k_{yyxy}, \tag{B.2e}$$

$$C_{xyxy} = C_{xxyy} + \frac{1}{64} \lambda_{xyxy}. \tag{B.2f}$$

Eqs. (B.2a)–(B.2c), Eqs. (B.2d)–(B.2e), and Eq. (B.2f) are actually three decoupled systems of equation. The solution of these systems of equations is shown in Eq. (30). Note that λ_{xyxy} appears only in the component C_{xyxy}, which is the component that would have been prescribed by the Cauchy's relation in a bond-based peridynamic formulation.

Appendix C. Computation of the components of the 3D elasticity tensor

Similarly to the 2D case, we will compute the PD components of the 3D elasticity tensor with Eq. (26) by considering a complete neighborhood. Thanks to the symmetry of the integration domain, the only non-null integrals that appear in Eq. (26) for a 3D peridynamic model are:

$$\int_{\mathcal{H}_{\mathbf{x}}} \frac{\omega(\|\boldsymbol{\xi}\|)}{\|\boldsymbol{\xi}\|^2} \xi_p^2 \xi_q^2 \mathrm{d}V_{\mathbf{x}'} = \frac{m}{15} \qquad \text{with } p, q = x, y, z \text{ and } p \neq q, \tag{C.1a}$$

$$\int_{\mathcal{H}_{\mathbf{x}}} \frac{\omega(\|\boldsymbol{\xi}\|)}{\|\boldsymbol{\xi}\|^6} \xi_p^8 \mathrm{d}V_{\mathbf{x}'} = \frac{m}{9} \qquad \text{with } p = x, y, z, \tag{C.1b}$$

$$\int_{\mathcal{H}_{\mathbf{x}}} \frac{\omega(\|\boldsymbol{\xi}\|)}{\|\boldsymbol{\xi}\|^6} \xi_p^6 \xi_q^2 \mathrm{d}V_{\mathbf{x}'} = \frac{m}{63} \qquad \text{with } p, q = x, y, z \text{ and } p \neq q, \tag{C.1c}$$

$$\int_{\mathcal{H}_{\mathbf{x}}} \frac{\omega(\|\boldsymbol{\xi}\|)}{\|\boldsymbol{\xi}\|^6} \xi_p^4 \xi_q^4 \mathrm{d}V_{\mathbf{x}'} = \frac{m}{105} \qquad \text{with } p, q = x, y, z \text{ and } p \neq q, \tag{C.1d}$$

$$\int_{\mathcal{H}_{\mathbf{x}}} \frac{\omega(\|\boldsymbol{\xi}\|)}{\|\boldsymbol{\xi}\|^6} \xi_p^4 \xi_q^2 \xi_r^2 \mathrm{d}V_{\mathbf{x}'} = \frac{m}{315} \qquad \text{with } p, q, r = x, y, z \text{ and } p \neq q \neq r, \tag{C.1e}$$

where m is the weighted volume (Eq. (13)). These integrals are solved by employing spherical coordinates.

By substituting the micromoduli in Eqs. (28) and (29) into the formula for the computation of the components of the PD elasticity tensor in Eq. (26) and using the solutions to the integrals in Eq. (C.1), we obtain the following system of equations:

$$C_{xxxx} = \frac{k_{xxxx}}{9} + \frac{k_{yyyy}}{105} + \frac{k_{zzzz}}{105} + \frac{k_{xxyy}}{63} + \frac{k_{xxzz}}{63} + \frac{k_{yyzz}}{315}, \tag{C.2a}$$

$$C_{yyyy} = \frac{k_{xxxx}}{105} + \frac{k_{yyyy}}{9} + \frac{k_{zzzz}}{105} + \frac{k_{xxyy}}{63} + \frac{k_{xxzz}}{315} + \frac{k_{yyzz}}{63}, \tag{C.2b}$$

$$C_{zzzz} = \frac{k_{xxxx}}{105} + \frac{k_{yyyy}}{105} + \frac{k_{zzzz}}{9} + \frac{k_{xxyy}}{315} + \frac{k_{xxzz}}{63} + \frac{k_{yyzz}}{63}, \tag{C.2c}$$

$$C_{xxyy} = \frac{k_{xxxx}}{63} + \frac{k_{yyyy}}{63} + \frac{k_{zzzz}}{315} + \frac{k_{xxyy}}{105} + \frac{k_{xxzz}}{315} + \frac{k_{yyzz}}{315}, \tag{C.2d}$$

$$C_{xxzz} = \frac{k_{xxxx}}{63} + \frac{k_{yyyy}}{315} + \frac{k_{zzzz}}{63} + \frac{k_{xxyy}}{315} + \frac{k_{xxyy}}{105} + \frac{k_{yyzz}}{315}, \tag{C.2e}$$

$$C_{yyzz} = \frac{k_{xxxx}}{315} + \frac{k_{yyyy}}{63} + \frac{k_{zzzz}}{63} + \frac{k_{xxyy}}{315} + \frac{k_{xxzz}}{315} + \frac{k_{yyzz}}{105}, \tag{C.2f}$$

$$C_{xxxy} = \frac{k_{xxxy}}{63} + \frac{k_{yyxy}}{105} + \frac{k_{zzxy}}{315}, \tag{C.2g}$$

$$C_{yyxy} = \frac{k_{xxxy}}{105} + \frac{k_{yyxy}}{63} + \frac{k_{zzxy}}{315}, \tag{C.2h}$$

$$C_{zzxy} = \frac{k_{xxxy}}{315} + \frac{k_{yyxy}}{315} + \frac{k_{zzxy}}{315}, \tag{C.2i}$$

$$C_{xxxz} = \frac{k_{xxxz}}{63} + \frac{k_{yyxz}}{315} + \frac{k_{zzxz}}{105}, \tag{C.2j}$$

$$C_{yyxz} = \frac{k_{xxxz}}{315} + \frac{k_{yyxz}}{315} + \frac{k_{zzxz}}{315}, \tag{C.2k}$$

$$C_{zzxz} = \frac{k_{xxxz}}{105} + \frac{k_{yyxz}}{315} + \frac{k_{zzxz}}{63}, \tag{C.2l}$$

$$C_{xxyz} = \frac{k_{xxyz}}{315} + \frac{k_{yyyz}}{315} + \frac{k_{zzyz}}{315}, \tag{C.2m}$$

$$C_{yyyz} = \frac{k_{xxyz}}{315} + \frac{k_{yyyz}}{63} + \frac{k_{zzyz}}{105}, \tag{C.2n}$$

$$C_{zzyz} = \frac{k_{xxyz}}{315} + \frac{k_{yyyz}}{105} + \frac{k_{zzyz}}{63}, \tag{C.2o}$$

$$C_{xyxy} = C_{xxyy} + \frac{\lambda_{xyxy}}{225}, \tag{C.2p}$$

$$C_{xzxz} = C_{xxzz} + \frac{\lambda_{xzxz}}{225}, \tag{C.2q}$$

$$C_{yzyz} = C_{yyzz} + \frac{\lambda_{yzyz}}{225}, \tag{C.2r}$$

$$C_{yzxz} = C_{zzxy} + \frac{\lambda_{yzxz}}{450}, \tag{C.2s}$$

$$C_{yzxy} = C_{yyxz} + \frac{\lambda_{yzxy}}{450}, \tag{C.2t}$$

$$C_{xzxy} = C_{xxyz} + \frac{\lambda_{xzxy}}{450}. \tag{C.2u}$$

Eqs. (C.2a)–(C.2f), Eqs. (C.2g)–(C.2i), Eqs. (C.2j)–(C.2l), Eqs. (C.2m)–(C.2o), Eq. (C.2p), Eq. (C.2q), Eq. (C.2r), Eq. (C.2s), Eq. (C.2t), and Eq. (C.2u) are actually ten decoupled systems of equation. The solution of these systems of equations is shown in Eq. (34).

References

[1] T. Ting, Anisotropic Elasticity: Theory and Applications, Vol. 45, Oxford University Press, USA, 1996, http://dx.doi.org/10.1093/oso/9780195074475.001.0001.

[2] J. Katz, A. Meunier, The elastic anisotropy of bone, J. Biomech. 20 (11–12) (1987) 1063–1070, http://dx.doi.org/10.1016/0021-9290(87)90024-8.

[3] J. Boutelje, The relationship of structure to transverse anisotropy in wood with reference to shrinkage and elasticity, 1962, http://dx.doi.org/10.1515/hfsg.1962.16.2.33.

[4] N. Barton, E. Quadros, Anisotropy is everywhere, to see, to measure, and to model, Rock Mech. Rock Eng. 48 (4) (2015) 1323–1339, http://dx.doi.org/10.1007/s00603-014-0632-7.

[5] J. Reddy, Mechanics of Laminated Composite Plates and Shells: Theory and Analysis, CRC Press, 2003, http://dx.doi.org/10.1201/b12409.

[6] Z. Li, G. Winther, N. Hansen, Anisotropy of plastic deformation in rolled aluminum, Mater. Sci. Eng. A 387 (2004) 199–202, http://dx.doi.org/10.1016/j.msea.2004.03.090.

[7] V. Azzi, S. Tsai, Anisotropic strength of composites: Investigation aimed at developing a theory applicable to laminated as well as unidirectional composites, employing simple material properties derived from unidirectional specimens alone, Exp. Mech. 5 (1965) 283–288, http://dx.doi.org/10.1007/BF02326292.

[8] J. Behiri, W. Bonfield, Fracture mechanics of bone—The effects of density, specimen thickness and crack velocity on longitudinal fracture, J. Biomech. 17 (1) (1984) 25–34, http://dx.doi.org/10.1016/0021-9290(84)90076-9.

[9] W. Bonfield, Advances in the fracture mechanics of cortical bone, J. Biomech. 20 (11–12) (1987) 1071–1081, http://dx.doi.org/10.1016/0021-9290(87)90025-X.

[10] J. Behiri, W. Bonfield, Orientation dependence of the fracture mechanics of cortical bone, J. Biomech. 22 (8–9) (1989) 863–872, http://dx.doi.org/10.1016/0021-9290(89)90070-5.

[11] S. Silling, Reformulation of elasticity theory for discontinuities and long-range forces, J. Mech. Phys. Solids 48 (1) (2000) 175–209, http://dx.doi.org/10.1016/S0022-5096(99)00029-0.

[12] S. Silling, M. Epton, O. Weckner, J. Xu, E. Askari, Peridynamic states and constitutive modeling, J. Elasticity 88 (2) (2007) 151–184, http://dx.doi.org/10.1007/s10659-007-9125-1.

[13] A. Agwai, I. Guven, E. Madenci, Predicting crack propagation with peridynamics: A comparative study, Int. J. Fract. 171 (2011) 65–78, http://dx.doi.org/10.1007/s10704-011-9628-4.

[14] J. Mehrmashhadi, M. Bahadori, F. Bobaru, On validating peridynamic models and a phase-field model for dynamic brittle fracture in glass, Eng. Fract. Mech. 240 (2020) 107355, http://dx.doi.org/10.1016/j.engfracmech.2020.107355.

[15] J. Trageser, P. Seleson, Bond-based peridynamics: A tale of two Poisson's ratios, J. Peridyn. Nonlocal Model. 2 (3) (2020) 278–288, http://dx.doi.org/10.1007/s42102-019-00021-x.

[16] S. Silling, Dynamic fracture modeling with a meshfree peridynamic code, in: Computational Fluid and Solid Mechanics 2003, Elsevier, 2003, pp. 641–644, http://dx.doi.org/10.1016/B978-008044046-0.50157-3.

[17] Y. Ha, F. Bobaru, Studies of dynamic crack propagation and crack branching with peridynamics, Int. J. Fract. 162 (2010) 229–244, http://dx.doi.org/10.1007/s10704-010-9442-4.

[18] Y. Ha, F. Bobaru, Characteristics of dynamic brittle fracture captured with peridynamics, Eng. Fract. Mech. 78 (6) (2011) 1156–1168, http://dx.doi.org/10.1016/j.engfracmech.2010.11.020.

[19] F. Bobaru, G. Zhang, Why do cracks branch? A peridynamic investigation of dynamic brittle fracture, Int. J. Fract. 196 (1–2) (2015) 59–98, http://dx.doi.org/10.1007/s10704-015-0056-8.

[20] Z. Xu, G. Zhang, Z. Chen, F. Bobaru, Elastic vortices and thermally-driven cracks in brittle materials with peridynamics, Int. J. Fract. 209 (2018) 203–222, http://dx.doi.org/10.1007/s10704-017-0256-5.
[21] A. Javili, R. Morasata, E. Oterkus, S. Oterkus, Peridynamics review, Math. Mech. Solids 24 (11) (2019) 3714–3739, http://dx.doi.org/10.1177/1081286518803411.
[22] S. Oterkus, E. Madenci, A. Agwai, Fully coupled peridynamic thermomechanics, J. Mech. Phys. Solids 64 (2014) 1–23, http://dx.doi.org/10.1016/j.jmps.2013.10.011.
[23] Y. Wang, X. Zhou, M. Kou, A coupled thermo-mechanical bond-based peridynamics for simulating thermal cracking in rocks, Int. J. Fract. 211 (1–2) (2018) 13–42, http://dx.doi.org/10.1007/s10704-018-0273-z.
[24] S. Bazazzadeh, M. Morandini, M. Zaccariotto, U. Galvanetto, Simulation of chemo-thermo-mechanical problems in cement-based materials with Peridynamics, Meccanica 56 (9) (2021) 2357–2379, http://dx.doi.org/10.1007/s11012-021-01375-7.
[25] Z. Chen, F. Bobaru, Peridynamic modeling of pitting corrosion damage, J. Mech. Phys. Solids 78 (2015) 352–381, http://dx.doi.org/10.1016/j.jmps.2015.02.015.
[26] S. Jafarzadeh, Z. Chen, F. Bobaru, Peridynamic modeling of repassivation in pitting corrosion of stainless steel, Corrosion 74 (4) (2018) 393–414, http://dx.doi.org/10.5006/2615.
[27] S. Jafarzadeh, Z. Chen, S. Li, F. Bobaru, A peridynamic mechano-chemical damage model for stress-assisted corrosion, Electrochim. Acta 323 (2019) 134795, http://dx.doi.org/10.1016/j.electacta.2019.134795.
[28] F. Vieira, A. Araújo, Implicit non-ordinary state-based peridynamics model for linear piezoelectricity, Mech. Adv. Mater. Struct. 29 (28) (2022) 7329–7350, http://dx.doi.org/10.1080/15376494.2021.1995798.
[29] F. Vieira, A. Araújo, A peridynamic model for electromechanical fracture and crack propagation in piezoelectric solids, Comput. Methods Appl. Mech. Engrg. 412 (2023) 116081, http://dx.doi.org/10.1016/j.cma.2023.116081.
[30] A. Vasenkov, Multi-physics peridynamic modeling of damage processes in protective coatings, J. Peridyn. Nonlocal Model. 3 (2) (2021) 167–183, http://dx.doi.org/10.1007/s42102-020-00046-7.
[31] D. Behera, P. Roy, E. Madenci, S. Oterkus, Prediction of thermal oxidation damage in polymers by using peridynamics, in: 2021 IEEE 71st Electronic Components and Technology Conference, ECTC, IEEE, 2021, pp. 1457–1463, http://dx.doi.org/10.1109/ECTC32696.2021.00232.
[32] F. Scabbia, C. Gasparrini, M. Zaccariotto, U. Galvanetto, A. Larios, F. Bobaru, Moving interfaces in peridynamic diffusion models and influence of discontinuous initial conditions: Numerical stability and convergence, Comput. Math. Appl. 151 (2023) 384–396, http://dx.doi.org/10.1016/j.camwa.2023.10.016.
[33] F. Scabbia, M. Zaccariotto, U. Galvanetto, F. Bobaru, Peridynamic simulation of elastic wave propagation by applying the boundary conditions with the surface node method, Mater. Res. Proc. 33 (2023) http://dx.doi.org/10.21741/9781644902677-51.
[34] E. Askari, J. Xu, S. Silling, Peridynamic analysis of damage and failure in composites, in: 44th AIAA Aerospace Sciences Meeting and Exhibit, 2006, p. 88, http://dx.doi.org/10.2514/6.2006-88.
[35] W. Hu, Y. Ha, F. Bobaru, Peridynamic model for dynamic fracture in unidirectional fiber-reinforced composites, Comput. Methods Appl. Mech. Engrg. 217 (2012) 247–261, http://dx.doi.org/10.1016/j.cma.2012.01.016.
[36] E. Oterkus, E. Madenci, Peridynamic analysis of fiber-reinforced composite materials, J. Mech. Mater. Struct. 7 (1) (2012) 45–84, http://dx.doi.org/10.2140/jomms.2012.7.45.
[37] E. Oterkus, E. Madenci, O. Weckner, S. Silling, P. Bogert, A. Tessler, Combined finite element and peridynamic analyses for predicting failure in a stiffened composite curved panel with a central slot, Compos. Struct. 94 (3) (2012) 839–850, http://dx.doi.org/10.1016/j.compstruct.2011.07.019.
[38] Y. Yu, H. Wang, Peridynamic analytical method for progressive damage in notched composite laminates, Compos. Struct. 108 (2014) 801–810, http://dx.doi.org/10.1016/j.compstruct.2013.10.018.
[39] D. De Meo, N. Zhu, E. Oterkus, Peridynamic modeling of granular fracture in polycrystalline materials, J. Eng. Mater. Technol. 138 (4) (2016) 041008, http://dx.doi.org/10.1115/1.4033634.
[40] Y. Hu, E. Madenci, Bond-based peridynamic modeling of composite laminates with arbitrary fiber orientation and stacking sequence, Compos. Struct. 153 (2016) 139–175, http://dx.doi.org/10.1016/j.compstruct.2016.05.063.
[41] W. Zhou, D. Liu, N. Liu, Analyzing dynamic fracture process in fiber-reinforced composite materials with a peridynamic model, Eng. Fract. Mech. 178 (2017) 60–76, http://dx.doi.org/10.1016/j.engfracmech.2017.04.022.
[42] Y. Azdoud, F. Han, G. Lubineau, A morphing framework to couple non-local and local anisotropic continua, Int. J. Solids Struct. 50 (9) (2013) 1332–1341, http://dx.doi.org/10.1016/j.ijsolstr.2013.01.016.
[43] M. Ghajari, L. Iannucci, P. Curtis, A peridynamic material model for the analysis of dynamic crack propagation in orthotropic media, Comput. Methods Appl. Mech. Engrg. 276 (2014) 431–452, http://dx.doi.org/10.1016/j.cma.2014.04.002.
[44] G. Zhang, G. Gazonas, F. Bobaru, Supershear damage propagation and sub-Rayleigh crack growth from edge-on impact: A peridynamic analysis, Int. J. Impact Eng. 113 (2018) 73–87, http://dx.doi.org/10.1016/j.ijimpeng.2017.11.010.
[45] J. Trageser, P. Seleson, Anisotropic two-dimensional, plane strain, and plane stress models in classical linear elasticity and bond-based peridynamics, 2019, http://dx.doi.org/10.48550/arXiv.1905.12761, arXiv preprint.
[46] N. Prakash, A general numerical method to model anisotropy in discretized bond-based peridynamics, J. Peridyn. Nonlocal Model. 4 (2) (2022) 257–302, http://dx.doi.org/10.1007/s42102-021-00078-7.
[47] A. Javili, A. McBride, P. Steinmann, Continuum-kinematics-inspired peridynamics. Mechanical problems, J. Mech. Phys. Solids 131 (2019) 125–146, http://dx.doi.org/10.1016/j.jmps.2019.06.016.
[48] A. Javili, S. Firooz, A. McBride, P. Steinmann, The computational framework for continuum-kinematics-inspired peridynamics, Comput. Mech. 66 (2020) 795–824, http://dx.doi.org/10.1007/s00466-020-01885-3.
[49] D. Tian, X. Zhou, A continuum-kinematics-inspired peridynamic model of anisotropic continua: Elasticity, damage, and fracture, Int. J. Mech. Sci. 199 (2021) 106413, http://dx.doi.org/10.1016/j.ijmecsci.2021.106413.
[50] W. Gerstle, N. Sau, S. Silling, Peridynamic modeling of concrete structures, Nucl. Eng. Des. 237 (12–13) (2007) 1250–1258, http://dx.doi.org/10.1016/j.nucengdes.2006.10.002.
[51] V. Diana, S. Casolo, A bond-based micropolar peridynamic model with shear deformability: Elasticity, failure properties and initial yield domains, Int. J. Solids Struct. 160 (2019) 201–231, http://dx.doi.org/10.1016/j.ijsolstr.2018.10.026.
[52] G. Shen, Y. Xia, P. Hu, G. Zheng, Construction of peridynamic beam and shell models on the basis of the micro-beam bond obtained via interpolation method, Eur. J. Mech. A Solids 86 (2021) 104174, http://dx.doi.org/10.1016/j.euromechsol.2020.104174.
[53] V. Diana, S. Casolo, A full orthotropic micropolar peridynamic formulation for linearly elastic solids, Int. J. Mech. Sci. 160 (2019) 140–155, http://dx.doi.org/10.1016/j.ijmecsci.2019.06.036.
[54] G. Shen, B. Xu, Y. Xia, W. Li, G. Zheng, A general anisotropic peridynamic plane model based on micro-beam bond, Comput. Mech. 71 (6) (2023) 1065–1079, http://dx.doi.org/10.1007/s00466-023-02274-2.
[55] Z. Li, Y. Lu, D. Huang, T. Rabczuk, Nonlocal anisotropic model for deformation and fracture using peridynamic operator method, Int. J. Mech. Sci. (2024) 109023, http://dx.doi.org/10.1016/j.ijmecsci.2024.109023.

[56] H. Zhang, P. Qiao, A state-based peridynamic model for quantitative elastic and fracture analysis of orthotropic materials, Eng. Fract. Mech. 206 (2019) 147–171, http://dx.doi.org/10.1016/j.engfracmech.2018.10.003.
[57] Y. Yu, S. Liu, S. Zhao, Z. Yu, The nonlinear inplane behavior and progressive damage modeling for laminate by peridynamics, in: ASME International Mechanical Engineering Congress and Exposition, 50510, American Society of Mechanical Engineers, 2016, V001T03A054, http://dx.doi.org/10.1115/IMECE2016-65821.
[58] G. Hattori, J. Trevelyan, W. Coombs, A non-ordinary state-based peridynamics framework for anisotropic materials, Comput. Methods Appl. Mech. Engrg. 339 (2018) 416–442, http://dx.doi.org/10.1016/j.cma.2018.05.007.
[59] W. Sun, J. Fish, P. Lin, Numerical simulation of fluid-driven fracturing in orthotropic poroelastic media based on a peridynamics-finite element coupling approach, Int. J. Rock Mech. Min. Sci. 158 (2022) 105199, http://dx.doi.org/10.1016/j.ijrmms.2022.105199.
[60] H. Wang, L. Wu, J. Guo, C. Yu, Y. Li, J. Wang, Z. Liu, Numerical analysis on failure of sheet metals with non-ordinary state-based peridynamics, Eng. Fract. Mech. 292 (2023) 109652, http://dx.doi.org/10.1016/j.engfracmech.2023.109652.
[61] H. Wang, L. Wu, J. Guo, C. Yu, Y. Li, Y. Wu, Three-dimensional modeling and analysis of anisotropic materials with quasi-static deformation and dynamic fracture in non-ordinary state-based peridynamics, Appl. Math. Model. 125 (2024) 625–648, http://dx.doi.org/10.1016/j.apm.2023.09.016.
[62] H. Chen, Bond-associated deformation gradients for peridynamic correspondence model, Mech. Res. Commun. 90 (2018) 34–41, http://dx.doi.org/10.1016/j.mechrescom.2018.04.004.
[63] H. Chen, B. Spencer, Peridynamic bond-associated correspondence model: Stability and convergence properties, Internat. J. Numer. Methods Engrg. 117 (6) (2019) 713–727, http://dx.doi.org/10.1002/nme.5973.
[64] F. Vieira, A. Araújo, On the role of bond-associated stabilization and discretization on deformation and fracture in non-ordinary state-based peridynamics, Eng. Fract. Mech. 270 (2022) 108557, http://dx.doi.org/10.1016/j.engfracmech.2022.108557.
[65] A. Love, A treatise on the mathematical theory of elasticity, 1892, URL: hal.science/hal-01307751.
[66] S. Silling, Linearized theory of peridynamic states, J. Elasticity 99 (1) (2010) 85–111, http://dx.doi.org/10.1007/s10659-009-9234-0.
[67] D. Littlewood, Roadmap for Peridynamic Software Implementation, Tech. Rep., Sandia National Laboratories, 2015, http://dx.doi.org/10.2172/1226115.
[68] Q. Le, W. Chan, J. Schwartz, A two-dimensional ordinary, state-based peridynamic model for linearly elastic solids, Internat. J. Numer. Methods Engrg. 98 (8) (2014) 547–561, http://dx.doi.org/10.1002/nme.4642.
[69] G. Ongaro, P. Seleson, U. Galvanetto, T. Ni, M. Zaccariotto, Overall equilibrium in the coupling of peridynamics and classical continuum mechanics, Comput. Methods Appl. Mech. Engrg. 381 (2021) 113515, http://dx.doi.org/10.1016/j.cma.2020.113515.
[70] S. Silling, R. Lehoucq, Convergence of peridynamics to classical elasticity theory, J. Elasticity 93 (1) (2008) 13–37, http://dx.doi.org/10.1007/s10659-008-9163-3.
[71] S. Silling, M. Zimmermann, R. Abeyaratne, Deformation of a peridynamic bar, J. Elasticity 73 (2003) 173–190, http://dx.doi.org/10.1023/B:ELAS.0000029931.03844.4f.
[72] Q. Le, F. Bobaru, Surface corrections for peridynamic models in elasticity and fracture, Comput. Mech. 61 (4) (2018) 499–518, http://dx.doi.org/10.1007/s00466-017-1469-1.
[73] F. Scabbia, M. Zaccariotto, U. Galvanetto, A novel and effective way to impose boundary conditions and to mitigate the surface effect in state-based peridynamics, Internat. J. Numer. Methods Engrg. 122 (20) (2021) 5773–5811, http://dx.doi.org/10.1002/nme.6773.
[74] F. Scabbia, M. Zaccariotto, U. Galvanetto, A new method based on Taylor expansion and nearest-node strategy to impose Dirichlet and Neumann boundary conditions in ordinary state-based Peridynamics, Comput. Mech. 70 (1) (2022) 1–27, http://dx.doi.org/10.1007/s00466-022-02153-2.
[75] S. Silling, E. Askari, A meshfree method based on the peridynamic model of solid mechanics, Comput. Struct. 83 (17–18) (2005) 1526–1535, http://dx.doi.org/10.1016/j.compstruc.2004.11.026.
[76] A. Shojaei, T. Mudric, M. Zaccariotto, U. Galvanetto, A coupled meshless finite point/peridynamic method for 2D dynamic fracture analysis, Int. J. Mech. Sci. 119 (2016) 419–431, http://dx.doi.org/10.1016/j.ijmecsci.2016.11.003.
[77] M. Zaccariotto, D. Tomasi, U. Galvanetto, An enhanced coupling of PD grids to FE meshes, Mech. Res. Commun. 84 (2017) 125–135, http://dx.doi.org/10.1016/j.mechrescom.2017.06.014.
[78] T. Ni, M. Zaccariotto, Q. Zhu, U. Galvanetto, Coupling of FEM and ordinary state-based peridynamics for brittle failure analysis in 3D, Mech. Adv. Mater. Struct. 28 (9) (2021) 875–890, http://dx.doi.org/10.1080/15376494.2019.1602237.
[79] F. Scabbia, M. Enea, An improved coupling of 3D state-based peridynamics with high-order 1D finite elements to reduce spurious effects at interfaces, Internat. J. Numer. Methods Engrg. (2023) http://dx.doi.org/10.1002/nme.7297.
[80] S. Jafarzadeh, A. Larios, F. Bobaru, Efficient solutions for nonlocal diffusion problems via boundary-adapted spectral methods, J. Peridyn. Nonlocal Model. 2 (1) (2020) 85–110, http://dx.doi.org/10.1007/s42102-019-00026-6.
[81] S. Jafarzadeh, L. Wang, A. Larios, F. Bobaru, A fast convolution-based method for peridynamic transient diffusion in arbitrary domains, Comput. Methods Appl. Mech. Engrg. 375 (2021) 113633, http://dx.doi.org/10.1016/j.cma.2020.113633.
[82] A. Shojaei, A. Hermann, C. Cyron, P. Seleson, S. Silling, A hybrid meshfree discretization to improve the numerical performance of peridynamic models, Comput. Methods Appl. Mech. Engrg. 391 (2022) 114544, http://dx.doi.org/10.1016/j.cma.2021.114544.
[83] G. Ongaro, A. Shojaei, F. Mossaiby, A. Hermann, C. Cyron, P. Trovalusci, Multi-adaptive spatial discretization of bond-based peridynamics, Int. J. Fract. (2023) 1–24, http://dx.doi.org/10.1007/s10704-023-00709-8.
[84] P. Seleson, Improved one-point quadrature algorithms for two-dimensional peridynamic models based on analytical calculations, Comput. Methods Appl. Mech. Engrg. 282 (2014) 184–217, http://dx.doi.org/10.1016/j.cma.2014.06.016.
[85] P. Seleson, D. Littlewood, Convergence studies in meshfree peridynamic simulations, Comput. Math. Appl. 71 (11) (2016) 2432–2448, http://dx.doi.org/10.1016/j.camwa.2015.12.021.
[86] F. Scabbia, M. Zaccariotto, U. Galvanetto, Accurate computation of partial volumes in 3D peridynamics, Eng. Comput. 39 (1) (2023) 959–991, http://dx.doi.org/10.1007/s00366-022-01725-3.
[87] E. Madenci, E. Oterkus, Peridynamic Theory and its Applications, vol. 17, Springer, 2014, http://dx.doi.org/10.1007/978-1-4614-8465-3.
[88] J. Zhao, S. Jafarzadeh, Z. Chen, F. Bobaru, An algorithm for imposing local boundary conditions in peridynamic models on arbitrary domains, 2020, http://dx.doi.org/10.31224/osf.io/7z8qr.
[89] F. Scabbia, M. Zaccariotto, U. Galvanetto, A new surface node method to accurately model the mechanical behavior of the boundary in 3D state-based peridynamics, J. Peridyn. Nonlocal Model. (2023) 1–35, http://dx.doi.org/10.1007/s42102-022-00094-1.
[90] J. Shewchuk, An introduction to the conjugate gradient method without the agonizing pain, 1994.
[91] Z. Chen, X. Peng, S. Jafarzadeh, F. Bobaru, Analytical solutions of peridynamic equations. Part II: Elastic wave propagation, Internat. J. Engrg. Sci. 188 (2023) 103866, http://dx.doi.org/10.1016/j.ijengsci.2023.103866.
[92] B. Okutan Baba, Behavior of pin-loaded laminated composites, Exp. Mech. 46 (2006) 589–600, http://dx.doi.org/10.1007/s11340-006-8735-z.
[93] C. Choy, W. Leung, K. Kowk, F. Lau, Elastic moduli and thermal conductivity of injection-molded short-fiber–reinforced thermoplastics, Polym. Compos. 13 (2) (1992) 69–80, http://dx.doi.org/10.1002/pc.750130202.